CRUSTAL STRUCTURE OF SOUTHWESTERN ANATOLIA USING P-RECEIVER FUNCTION ANALYSIS

by

Yaman Özakın

B.S., Physics, Boğaziçi University, 2004

Submitted to the Kandilli Observatory and Earthquake
Research Institute in partial fulfillment of
the requirements for the degree of
Master of Science

Graduate Program in Geophysics Department
Boğaziçi University

2008

CRUSTAL STRUCTURE OF SOUTHWESTERN ANATOLIA
USING P-RECEIVER FUNCTION ANALYSIS

APPROVED BY:

Prof. Mustafa Aktar . . . . . .
(Thesis Supervisor)

Assoc. Prof. Hayrullah Karabulut . . . . . .

Assoc. Prof. Serdar Özalaybey . . . . . .

Assoc. Prof. Nurcan Özel . . . . . .

DATE OF APPROVAL: 21.January.2008

This Thesis is dedicated to my dear friend, Sinem.

TABLE OF CONTENTS

ACKNOWLEDGEMENTS

I would like to express my gratitude to Professor Mustafa Aktar for his patience, encouragement and friendship. Without his help, I wouldn't be able to go on during times when everything seemed desperate.

I would also like to thank Dean Childs for his tutorship on fieldwork and all the work he has done which made data for this thesis available.

Also I would like to mention the help and care I got from my friends in Kandilli Observatory Geophysics Department, who help me to adapt to the world of earth sciences.

ABSTRACT

CRUSTAL STRUCTURE OF SOUTHWESTERN ANATOLIA USING P-RECEIVER FUNCTION ANALYSIS

The crustal structure in Aegean has been subject to many geophysical studies. To enlarge the picture of Aegean and African Moho's, a P receiver function analysis has been conducted on data collected for 15 months from 12 seismic stations in south-western Anatolia. The results agree with that of various geophysical studies made on the same area. The calculated Moho depth increases from 20 km.'s in FETY, which is due to the south of Gökova Bay, to 29.4 km. in MLSB, which is due to the north of the bay. The trend of the slope appears to be in the NW-SE direction. In stations located on the southern side of the Gökova Bay, it is also possible to observe a second conversion phase which is attributed to Moho of African plate. The slope of the Moho of the African plate appears to follow the NE-SW line in the region.

ÖZET

ALICI FONKSİYONLARI KULLANARAK HESAPLANAN GÜNEY-BATI ANADOLU KABUK YAPISI

Ege'nin karmaşık kabuk yapısı, uzun zamandır araştırmacıları üzerinde yoğun araştırmalar yapmaya itmiştir. Tomografi, yüzey dalgası analizi, kırınma profili gibi tekniklerle bölge hakkında genel bir takım bilgiler edinilmişse de ayrıntılı kabuk yapısını anlamak için alıcı fonksiyon teknikleri kullanılana kadar çarpıcı bir sonuç alınamamıştır. Bölgede bu teknikle yapılan çalışmalar da Ege Denizinin ayrıntılı yapısını çıkarmayı başarmış ama Ege denizinin kıyı şeridinin doğusu araştırma alanının dışında kaldığından bilinmezliğini korumuştur. Bu çalışmada yoğun olarak Gökova Körfezi'nin çevresinde kurulu deprem istasyonlarından alınan verilerle alıcı fonksiyonları tekniği uygulanarak kabuk kalınlığı haritası çıkarılmış, Ege plakasının Moho süreksizliğinin kuzey-batı yönünde derinleştiği, altında kalan Afrika plakasının Moho süreksizliğin ise güney-batı yönünde derinleştiği gözlemlenmiştir. Diğer çalışmalarla kesişen bölgelerdeki kabuk yapısına ait bulgular birbiriyle örtüşmektedir.

LIST OF FIGURES

LIST OF TABLES

LIST OF SYMBOLS

H	Thickness of the velocity discontinuity
K	Poisson's ratio
p	Ray parameter
Tps	Delay time of Ps phase
Tpppps	Delay time of PpPs phase
Vp	P-wave velocity
Vs	S-wave velocity

1. INTRODUCTION

The complex structure of Aegean puzzled the researchers for many years. Its location is in the middle of three converging tectonic plates (Eurasia, Africa and Anatolia) and it has been subjected both to compression and also extension successively. The southern part of Aegean is completely dominated by the subduction of whatever remains from the Thetis Ocean and is often referred as the African subduction. A geological history which includes intermittent stages of compression and extension resulted in current structure of Aegean. The principal reasons for extension and its magnitude are still a subject of debate (McKenzie, 1972; Le Pichon and Angelier, 1979; McKenzie, 1978; Gautier *et al.*, 1999).

Gaining more insight of the underlying structure of Aegean, the crust and the lithosphere plays a key role in proving or disproving current theories about Aegean. In the past, many geophysical surveys were carried out to reveal the detail of the deeper structure, among which surface wave studies (Karagianni *et al.* 2005; Bourova *et al.*, 2005), seismic tomography (Spakman, 1986; Spakman *et al.*, 1988; Drakatos and Drakopoulos, 1991; Spakman *et al.*, 1993; Papazachos *et al.*, 1995; Papazachos and Nolet, 1997), marine seismics (Makris, 1973, 1978; Makris and Stobbe, 1984; Delibasis *et al.*, 1988; Bohnhoff *et al.*, 2001; Clement *et al.*, 2004), and gravity (Le Pichon and Angelier, 1979; Makris and Stobbe, 1984; Tsokas and Hansen, 1997; Tiberi *et al.*, 2001; Tirel *et al.*, 2004) provided many useful information but failed to provide detailed images of the exact depth and the variations of the Moho discontinuity.

The subducting plate was somehow imaged down to the depth of 600 km, extending nearly from the South of Crete to below the northern Aegean. It was also shown that the dip of the subducting plate increases as we go from west to east, giving therefore a kinked form (Hatzfeld, 1989; Papazachos and Nolet, 1997). However the exact effect of the subduction on the shallower structures that lay above, is not well observed.

Receiver function method was found to be the most sensitive method for providing an estimate for the Moho depth. It provides travel time from deep crustal and lithospheric discontinuities with consistency if enough data is available. However since the receiver

function only provides the travel time from the discontinuity, the absolute crustal velocity needs to be known in order to convert the time into depth. Scientist have used surface wave analysis together with the receiver function method in order to estimate the crustal velocities (Ozalaybey *et al.*, 1997). However, in situations where crustal velocities are not available or diffucult to estimate accurately, it is also a common practice to assume an average values for the crustal velocity as well as the Poisson Ratio (Soudoudi *et al.*, 2006).

Provided large number of events is analyzed with receiver function analysis, mapping of crustal and sub-crustal velocity discontinuities is easily achieved. In recent years many studies were conducted on the Aegean Sea, especially around the Island of Crete. It was observed that nowhere on any of the Aegean islands a very thick crust is observed. Conversely no observation was made that will imply a significant thinning of the crust as one would expect from an extension zone.

Li *et al.* (2003) conducted a receiver function study in the area around Crete which revealed a complex crustal structure beneath the Island. The crust thickness was however close to a normal continental crust, therefore showing no sign of any compression or extension. However he pointed out that the western stations showed a negative velocity contrast at Moho indicating a high degree of serpentinization in the upper Mantle. Furthermore region just north of the Crete, around the island of Thera, showed a high degree of anisotropy in the crust but also with a normal crustal depth.

More recently, Sodoudi et al (2006) made a detailed work about Aegean using P and S receiver functions. Her study revealed many aspects of the structure of Aegean and African Moho's particularly she showed that receiver funcitons detected no sign of any subducting plate below the depth of 200-250 km (delay time about 20 s). Her area of study does not extend to southwestern Anatolia, which is the focus of this study.

Stations deployed for the study of Gökova bay and its seismic structure proved to provide useful data for a receiver function study. By including also some of the BU Kandilli Observatory and Earthquake Research Institute online seismic stations (MLSB, BODT, DAT0, BLCB, ELL, and others) most of the southwestern Anatolia has been covered, however scarcely except Gökova region which has the most dense network.

The aim of this study is to image the crustal structure of Aegean and African plates beneath the South-western Anatolia using P-receiver functions calculated from seismograms of 12 offline and online stations. The resulting Moho depth map agrees with most of the other geophysical studies made on the same area.

A highly automated analysis method is developed throughout the analysis stage of the study, which makes it possible to conduct other receiver function studies without spending too much time.

The parts of this thesis are as following:

Chapter 2 is an overview of Geology of Aegean. Different studies are compared and the idea of microplates in the region is explained.

Chapter 3 is the explanation of the method of P receiver function technique and method of determining K and H using receiver functions.

Chapter 4 gives the results of the receiver function analysis of 12 stations with figures of receiver functions and calculation of K and H for each station. Moho maps are displayed which were calculated using the Moho depth values.

Chapter 5 discusses the results and compares them with other studies.

2. GEODYNAMICS OF THE AEGEAN LITHOSPERE AND ITS DEEP STRUCTURE

2.1. Geological Setting

The evolution of the Aegean Region was always the focus of intense studies in the earth science community due to the wide variety of geological features of great interest, such as subduction, lithospheric stretching, rifting, volcanism, and many others. The complex history of the Aegean started probably during the Late Cretaceous (McKenzie, 1972). It first showed a stage compression driven by the NS convergence of African and Eurasian plates which was then followed by a period of NS extension, still continuing today. The exact timing for the initiation of the extension is matter of ongoing debate and probably varies with the location (Gautier *et al.*, 1999). In western Anatolia, it is dated between 20-14 Ma, based on the radiometric dating of the metamorphic rocks that constitute the core of the Menderes Massif (Seyitoğlu and Scottt, 1996).

The magnitude and the causes of the extension are also a subject of debate. Some authors argue that the extension is caused by subduction of African plate underneath the Aegean plate and therefore is related to the slab pull (McKenzie, 1978; LePichon and Angelier, 1979). Others relate the extension to the westward expulsion of the Anatolia due to the Eurasia-Arabia collision (McKenzie, 1978; Dewey and Şengör, 1979).

The subduction of the African plate beneath Eurasian plate is still continuing at a low rate and with a low angle. The subduction zone corresponds to the western half of the Hellenic trench which starts in Peloponnesus Peninsula on the west and reaches as far as southern coast of Anatolia. The eastern half of the trench is a left lateral strike slip transform zone. The exact deeper geometry of the subducting plate is not known although both seismic tomography (Papazachos and Nolet, 1997) and receiver function studies (Soudoudi *et al.*, 2006) provide images of the plunging plate. The traces of the subducting plate can be traced as far as northern shores of Aegean Sea (Sodoudi *et al.*, 2006).

The Western Anatolia, in particular, exposes many of the characteristic features of the Aegean extensional regime. The topography includes grabens most of which are perpendicular to the direction of extension of the plate, i.e. elongated in the EW direction. A high heat flow can be observed which again is due to the extension related thinning. (McKenzie, 1971; Mercier et. al., 1977; Jackson *et al.*, 1994).

2.2. Plate Tectonics Interpretation

Pioneering studies on the Aegean, focusing on the widespread young magmatism, increased heat flow, and particularly on earthquake mechanisms showing abundant normal faults, lead to the identification of it, as a distinct plate subject to an intense stretching (McKenzie, 1978). Average properties were then attributed to the total area that constitute the Aegean Plate, such as an average crustal thickness, and average extension rate, an average heat flow rate, etc. However, as detailed studies were made, it was noticed that most of the observations failed to verify the inferred average properties. It was immediately clear that, it was not correct to think of the Aegean as a homogeneous plate where general properties are evenly distributed over the total plate. Instead one had to think of a plate where the most prominent dynamic features are concentrated in limited local zones while the rest continues to behave like a normal non-deforming plate. In fact, there is convincing evidence that the region is formed by an assembly of microplates of which the exact number and boundaries is an area of active research. (Nyst and Thatcher, 2004; Aktar *et al.*, 2007).

In that direction the GPS surveys provides a data with unprecedented resolution and coverage. According to recent GPS studies, it is becoming convenient to consider the Aegean, not as a single plate but a region which contains four distinct microplates as in figure 2.1 (Nyst and Thatcher, 2004). The tectonic framework of the region is dominated by interaction of these four microplates and the subduction of African plate. Euler vectors of the current motion of the plates are given in the table below (Table 2.1). Broadly speaking, Aegean region is defined as being bounded by central Greece and south Marmara microplates in the north, Anatolian plate in the east and African plate in the south (Nyst and Thatcher, 2004). It would then be more logical to refer to general properties of the individual microplates. According to the classification of the microplate given by Nyst

and Thatcher (2004) the South Aegean Microplate is best to characterize the intense stretching that is expected to occur in the whole region. It should also be noted that three pieces of lands that best represents the South Aegean Microplate, are the Peloponnese Peninsula, Crete and the small portion of the South West Turkey around the Gokova Bay.

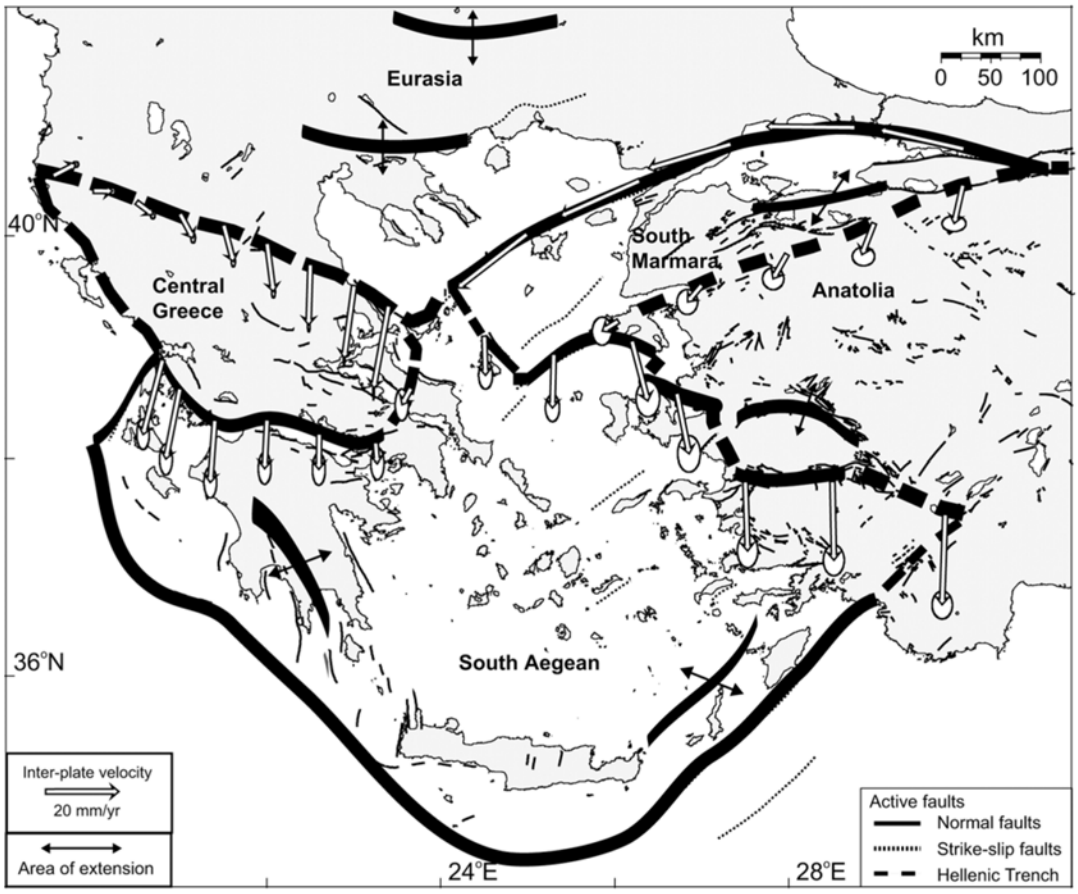

Figure 2.1. The microplate model (Nyst and Thatcher, 2004)

Table 2.1. The Euler Vectors of microplates (Nyst and Thatcher, 2004)

Region	Euler Vectors			MF1	MF2	MF3
	Latitude, °N	Longitude, °E	Rotation Rate, °/Myr			
Central Greece[b]	39.78 ± 0.02	19.99 ± 0.06	4.34 ± 0.10	2.3	2.1	2.2
South Aegean[b]	−45.91 ± 0.05	161.77 ± 3.61	0.52 ± 0.03	3.7	1.9	2.0
Anatolia[c]	−30.7 ± 0.8	32.6 ± 0.4	1.2 ± 0.1	2.1	1.7	1.8
				10.4[d]	8.6[d]	8.1[d]
South Marmara[c]	36.10	28.68	2.50	2.4	2.0	1.7
				6.0[d]	4.9[d]	3.2[d]

2.3. Study of the Deep Structure of the Aegean

To study the deep structure of Aegean, various studies were made using traveltime analysis (Panagiotopoulus and Papazachos, 1985), refraction profiles (Makris, 1973, 1978; Makris and Stobbe, 1984; Delibasis *et al.*, 1988; Bohnhoff *et al.*, 2001; Clement *et al.*, 2004) and tomographic studies (Spakman, 1986; Spakman *et al.*, 1988; Drakatos and Drakopoulos, 1991; Spakman *et al.*, 1993; Papazachos *et al.*, 1995; Papazachos and Nolet, 1997). Among these, only tomographic studies produced a rather large and homogeneous picture. But the intrinsic limitations of tomography techniques, which makes deciding between thin and slow crust and thick and fast crust difficult, gave only a broad picture.

Receiver function studies provided a useful tool for understanding the deep structure of the Aegean region.

Knapmeyer and Harjes carried out a very detailed study of the deep structure of western Crete. Although the observation period was limited and they only used P-receiver functions, the high number of stations densely located in a relatively small area allowed them to use advanced seismic processing tools, including migration. They succeeded in obtaining a high spatial resolution for this relatively small area. They detected two discontinuity zones: a shallow and non-dipping one gently ondulating between 15 and 20 km, and a deeper one dipping ESE, between 40 and 70 km. They associated the upper one with the thin continental crust of the Aegean and the deeper one with the subducting African Moho. They proposed that a fossil accretionary prism of thickness of 20-30 km, filled the space in between.

Li *et al.* used data from high quality stations (STS-2) installed with a wider coverrage, in Crete as well as to the south (Gavdos Island) and to the north (Santorini, Naxos, Samos Islands). Their receiver function in Crete showed no positive Moho conversion, which they interpreted as being due to lower shear wave velocity of the serpentinized forearc Mantle. Using the negative conversion peak they located the Moho depth to 32 km. A later conversion at 7 sec, corresponding to 63 km, they interpreted as the subducting African Moho, consistent with Knapmeyer and Harjes. South of Crete, Gavdos showed a thinner crust (26 km) and shallower subducting Moho (44 km). Beneath

Santorini Island, Aegean and subducting Moho were located to 32 and 99 km respectively, with a strong crustal anisotropy. The northern stations showed Moho depth of the order of 30 km or less, with a weak trace of subducting Moho. They proposed that Crete can be considered as a separate microplate on top of the Benioff zone.

Endrun *et al.* processed data from dense array of stations located in central and western Crete. They obtained velocities using surface wave analysis. Their results partly confirmed earlier ones obtained by Knapmeyer and Harjes and Li *et al.* Contrary to Knapmeyer and Harjes they detected no Moho in the western Crete, but confirmed the 30 km Moho for the central Crete suggested by Li *et al.* The African Moho was roughly located to 55 km beneath Crete, not contradicting previous studies.

Sodoudi *et al.* made a detailed study on data obtained from Aegean sea, Greece and Crete, which gave a detailed picture of the crust and lithosphere of Aegean and subducted African plate. Most remarkable results are the map of Moho of Aegean which revealed its depth as 25-33 km beneath Crete and 25-28 km beneath Peloponnessus. A rather unexpected result was the fact that observation of African plate even beneath the northern Greece which revealed the very low angle of subduction.

Recent studies made in the Menderes Graben (Zhu and Akyol, 2005) revealed a crustal thickness of 30 km. in the average, which is thicker than what would have been expected for a region where the stretching factor is expected to reach a level of 50% (Şengör *et al.*, 1984).

It is likely that intense stretching occurred locally in some parts while others patches of unstretched blocks kept their initial crustal thicknesses. At this stage it becomes clear that measuring the crustal thickness at a denser grid interval becomes the most critical tool for testing the various hypothesis related to the extension process.

This study aims to cover the area where the study area of Sodoudi *et al.* (2006) ends, therefore revealing the structure of Aegean and Africa beneath SW Anatolia. The results may help to have a better understanding of the ongoing tectonic processes of Aegean and African plate and gain insight about the extensional regime of Aegean.

3. RECEIVER FUNCTION METHOD

3.1. Pioneering Studies for Receiver Functions

Receiver Function Analysis method was first used by Burdick and Langston in 1977. They noticed that some energy in SV component of the receiver can be observed near the P wave arrival times. They concluded that it was the result of a conversion caused by a velocity discontinuity near the receiver. The method they used at the time was forward modeling of waveforms for different crustal velocity structures to obtain the wave forms similar to the ones observed.

In 1991, an inversion method was introduced by Charles J. Ammon which enabled seismologists to find the velocity structures without apriori knowledge of local velocity discontinuities. The method involved spectral deconvolution technique with water level of Clayton and Wiggins (Clayton and Wiggins, 1976).

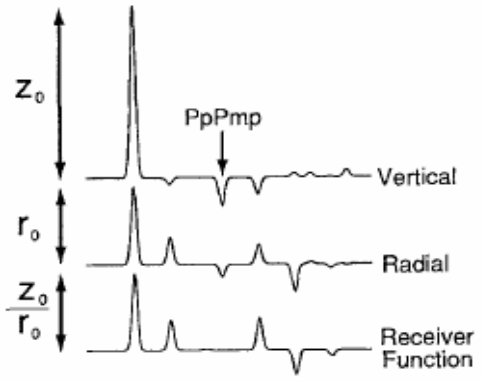

Figure 3.1. Vertical and radial response and the receiver function calculated for a single layer above a half space. The amplitude relationship between the synthetic response and the receiver function is indicated to the left of the traces. (Ammon, 1991)

By deconvolving the radial component from vertical, a waveform whose peaks indicate positive or negative velocity contrasts has been found. Since it indicates the structure near the receiver, it is called a “Receiver Function” (Figure 3.1).

In 1999, Ammon also developed a time domain inversion technique called “iterative time domain deconvolution” which gave better results for data with high signal to noise ratio. Today, this technique is the most widely used technique for estimating receiver functions.

Receiver Functions are used to study Moho depths and subduction zones and other complex structures. In order to get a clear picture of the area studied, one needs a good coverage of seismic stations and high quality data. The number of events is also an important factor. For offline studies data collection should be long enough to cover a large number of events.

The second phase of receiver function analysis is converting the arrival times of converted phases to depths. Some of the methods to do that are Joint Inversion of Receiver Function with Surface Wave Dispersion, method of 2D grid scan (Zhu and Kanamori, 2000), method of Zhu (Zhu *et al.*, 2006).

Joint inversion of receiver functions with surface wave dispersion data requires rather large amount of processing and work. The other two methods use information which is already inside the receiver function. Method of Zhu and Kanamori is appealing in the sense that it gives a clear peak for each receiver function. The trouble with that method is that it is dependent on some coefficients of which the values are determined by trial and error.

The method of Zhu *et al.* (2006) uses the arrival time of Ps phase which should be picked by hand for each waveform. After this step, most probable values of H and K are determined by selecting a peak in the resulting function in the appropriate range.

The method of Zhu and Kanamori is more compatible with automated processing schemes since it requires no picking and minimum amount of organizing. Hence it is used today in the automated receiver function analysis programs.

3.2. Receiver Function Analysis Techniques

3.2.1. Mathematical Description of Receiver Function

A receiver function is the impulse response of the seismic velocity structure underlying the seismic station when excited by a seismic event. It is computed by deconvolving the radial component from the vertical component of seismic data. The deconvolution can be made either in time domain or in frequency domain.

Suppose P(t) is the direct P wave of a teleseismic event. When the traveling seismic signal reaches a seismic velocity discontinuity between two homogeneous layers at an oblique angle, it will split into P-wave and SV-wave, of which the latter one will reach the station later than the former.

The ratio of energy in P-wave to converted SV-wave depends on the angle of incidence of initial P-wave. The closer the incident rays angle to perpendicular to the interface between the layers, smaller is this ratio.

If a 1D model is assumed, it is possible to conclude that all the converted energy from P wave will be in the horizontal component of the receiver.

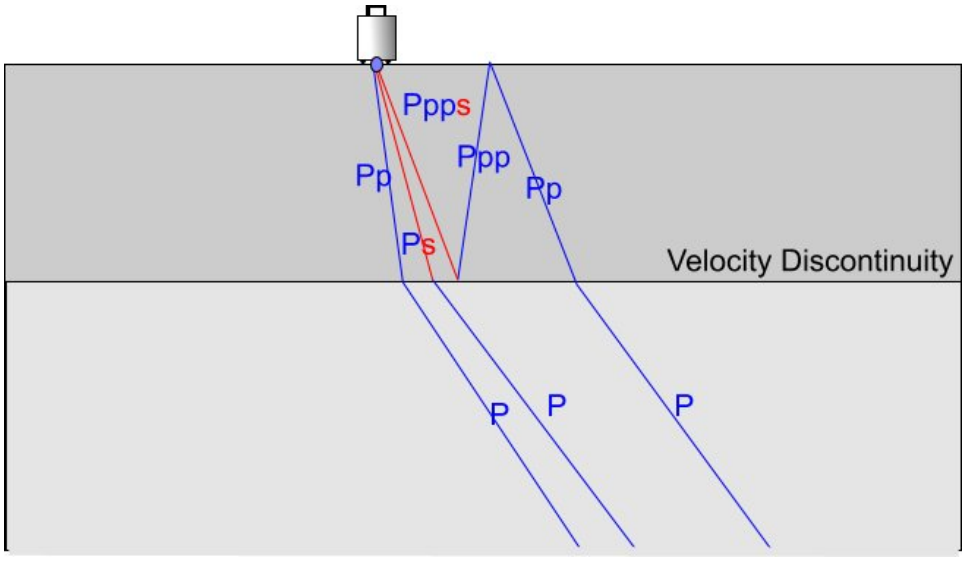

Figure 3.2 . The phase transitions of an incoming teleseismic event.

Earthquake signals from distant events carry information about the source, the path of the signal and Lithospheric and crustal structure near the receiver. To extract the information about the structure near the receiver, studying the S waves caused by refractions at a velocity discontinuity is a suitable analytic method.

Let the original signal in frequency domain from a teleseismic event in radial component be E(w), all the change which the signal goes through on its path be T(w), the instrument response I(w), and response to local velocity contrast near the receiver F(w).

The signal recorded in vertical component will be

$$Z(\omega) = E(\omega)T(\omega)I(\omega) \tag{3.1}$$

The radial component at the receiver relative to the events location will be,

$$R(\omega) = E(\omega)T(\omega)I(\omega)F(\omega) \tag{3.2}$$

So, to find the function which represents the local velocity contrast, we must divide the radial component of the seismogram by the vertical component.

$$F(\omega) = \frac{R(\omega)}{Z(\omega)} \tag{3.3}$$

This corresponds to a deconvolution in time domain. The inverse Fourier Transform of function, $F(t)$ is called the Receiver Function and indicates the velocity contrast on the path of the incoming seismic ray.

The division in frequency domain corresponds to a deconvolution in time domain. So calculating $F(w)$ in frequency domain is actually a deconvolution problem.

The deconvolution can be calculated either in time domain or in frequency domain.

So the problem of calculating the Receiver Function is a problem of deconvolution. There are various types of deconvolution techniques but the most well known ones for the Receiver Function estimation are:

(i). Spectral Domain Deconvolution with Water Level,
(ii). Iterative Time Domain Receiver function calculation.

Brief descriptions of both methods are discussed in the following section.

3.2.2. Receiver Function Estimation Techniques

3.2.2.1. Spectral Domain Deconvolution with Water Level. Water level deconvolution technique is the direct solution to the equation (3.3). For purpose, the radial and horizontal components of the seismograms need to be transformed into frequency domain using Fourier Transform.

Once the components are transformed, result of division of them yields the receiver function. To calculate the division of a number by a complex number, the denominator should be a real number which could be accomplished by multiplying both nominator and denominator by the conjugate of denominator which is indicated with (*) below.

$$R(\omega) = \frac{H(\omega)}{V(\omega)} \tag{3.4}$$

$$R(\omega) = \frac{H(\omega)V^*(\omega)}{V(\omega)V^*(\omega)} \tag{3.5}$$

In the operation (3.4) the divider term may take very small values for certain sections of the frequency spectrum where it can practically be assumed to be zero. To avoid the problem of division by very small numbers, the values of the Fourier transforms of the functions below some certain value called “Water Level Value” are replaced with it.

The advantages of this technique are that it is fast and relatively simple. The drawback is that it might give false bumps in receiver function which are not a result of a velocity contrast in seismograms of stations in which the signal to noise ratio is high.

3.2.2.2. Iterative Time Domain Receiver Function Estimation. Iterative time domain deconvolution technique (Ligorria, Ammon, 1999) assumes that the receiver function consists of superposition of multiple impulses. In practice since impulses imply infinite frequency range, a bandlimitied version of the impulses are used which, in most cases, are pulses of gaussian shape. The location of the individual gaussians is calculated by cross correlating the two components and finding the time of the first peak in the correlated function. Then the result is convolved with the Z component and subtracted from the original R component. The result is then again cross correlated with Z component. This process is repeated as many times as desired number of spikes in the receiver function.

This process is slower than water level deconvolution but gives better results even if the initial data has relatively low signal to noise ratio.

A pulse in the receiver function indicates a velocity discontinuity on the arriving rays path. The location of the pulse is correlated with the distance of the discontinuity from the receiver. Since S waves travel slower than P waves, the farther the distance where both Ps and P phases are present at the same time, the larger the delay between the arrival times of the two.

Each positive gaussian pulse indicates a sudden decrease in the velocity on the rays path to the receiver. The amplitude of the pulse increases as the ratio of the energy in SV component to the energy in P component increases. This can be due to the angle of incidence of the incoming ray, sharpness of the velocity contrast or both.

Besides the direct arrivals of the converted phases, there are also rays which are reflected once or more between the surface and a velocity discontinuity. Usually the multiples due to the Moho discontinuity arrive around 12 seconds. This makes it difficult, often impossible to observe any velocity contrasts of which the arrival of their converted phases coincides with the arrival of multiples of Moho.

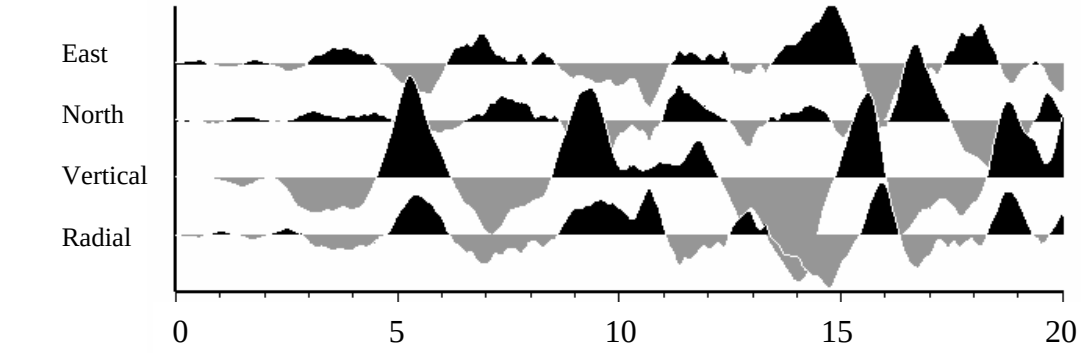

(a)

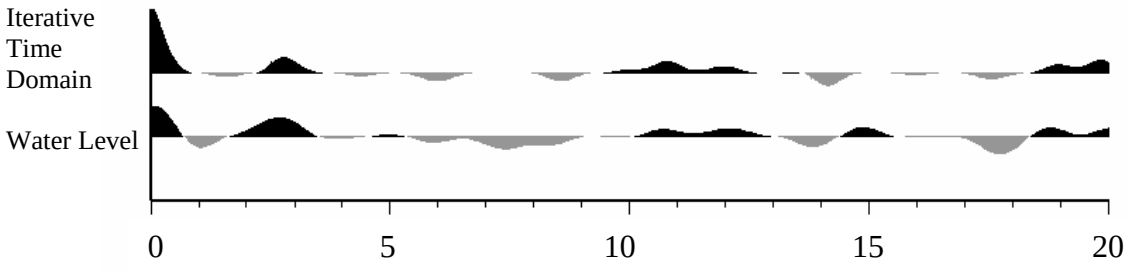

(b)

Figure 3.3. (a) The East, North and vertical components of a seismogram recorded in BLCB during a teleseismic event. (b) The results of two different techniques of receiver function estimation.

3.2.3. Kappa / Depth Problem

After identifying the peak which represents Moho conversion in the receiver function waveform, the depth of the Moho discontinuity should be calculated. The receiver function only gives the delay time between P wave and converted S wave. Converting the delay time to depth requires some knowledge of the Vp/Vs ratio which will be referenced as K throughout this text. If such knowledge is not present, the arrival times of the multiples can be used to constrain K and H.

Different K and H value couples can result in the same Tps arrival time. The same is true also for any Tppps arrival time. But there is only one solution of K and H for certain Tps and Tppps values.

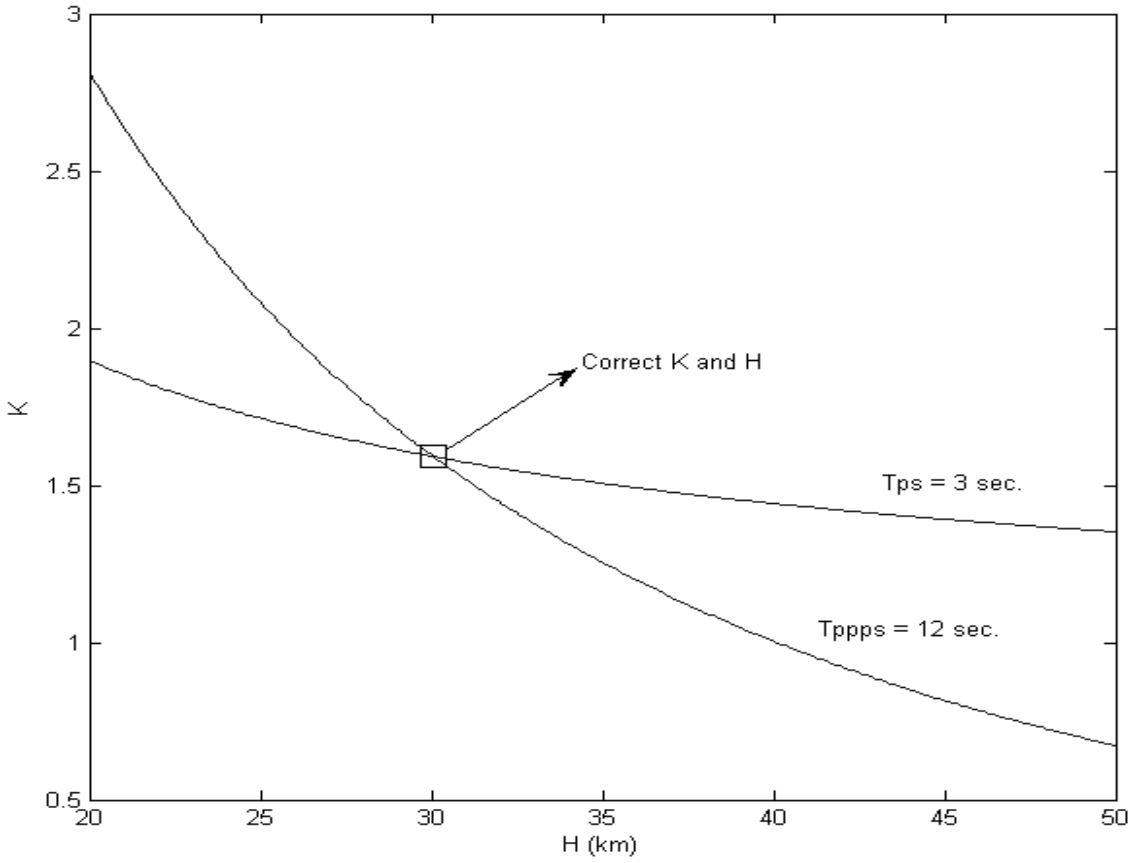

Figure 3.4. Curves, which indicate possible values of K for different values of H given a certain amount of Tps and Tppps time. The intersection is the solution of depth velocity discontinuity estimation problem for a receiver function with arrival times Tps and Tppps.

There are many methods for estimating the Poisson Ratio. Three methods are described below. The first one corresponds to the most conventional, but the less sensitive one (Zhu and Kanamori, 2000). The second one is a recent one proposed by Zhu *et al.* (2006) and is on the way of becoming the most popular one, due to the the improved sensitivity. The last one is a novel one developed within the framework of this thesis. The multiples resulted from arrivals of rays with different incidence angles results in receiver functions with spread arrivals of multiples. This method is an extension of the former one (Zhu *et al.,* 2006) but improves the estimation process by taking into account spurious fluctuation of the gaussian peaks of the multiples. These fluctuations may be due to noise in data, inclination or irregularity of the Moho interface, and high variation of the incidence angle of the incoming wave.

3.2.3.1. H-K Stacking (2D Grid Search). This method consists of examining the values that the receiver functions take at two critical times which corresponds to the arrival of Ps and Ppps phases for various choices of H and K values. For that purpose all receiver functions are first stacked to obtain one single waveform to represent the final receiver function. Ps and Ppps arrival times are calculated for a pair of H and K values, and a test is made to decide whether the representative receiver function has actually two peaks at these arrival times. In order to combine the contribution from both Ps and Ppps into single scalar value, the value of the stacked receiver function at these predicted arrival times are premultiplied by weighting coefficients and added together. This process is repeated for a grid of H-K pairs to obtain a 3D-plot. The third dimension plotted over H-K space gives the measure of the joint contribution of the Ps and PpPs amplitudes of the stacked receiver function at each H-K pairs (Zhu and Kanamori, 2000).

The result is a 3D surface with a peak at the most appropriate value pairs of H and K.

Since the multiplied constants are selected on subjective grounds and have a rather large effect on the resulting surface, this method can be considered to be biased.

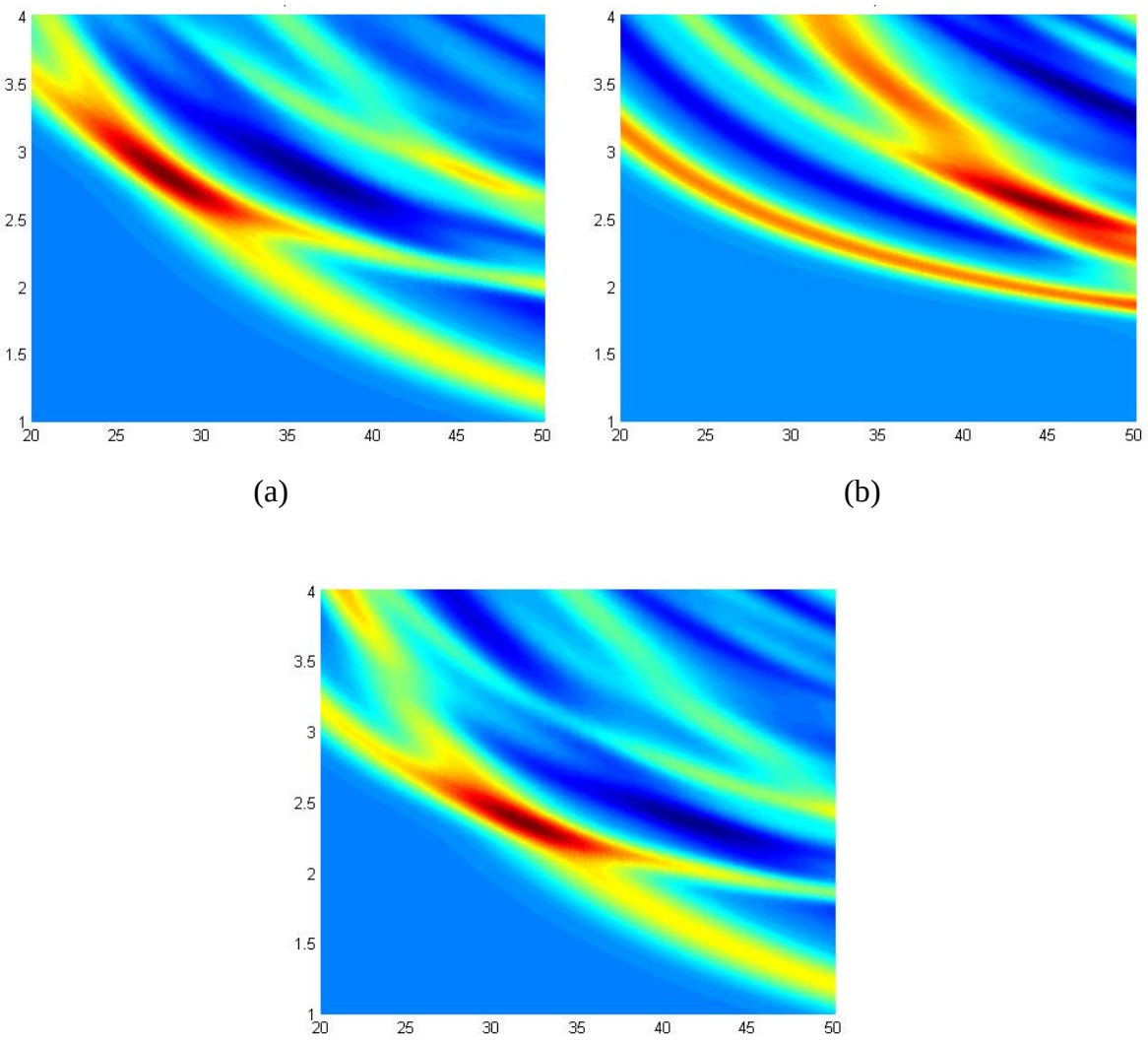

(a) (b)

(c)

Figure 3.5. The surface calculated by Zhu and Kanamori's method using the receiver function of a real event. The dark spots indicate the most appropriate H and K value for given W1 and W2 values. Slight differences in these coefficients result in significantly different outcomes. (a) W1 = 0.6, W2 = 0.3, (b) W1 = 0.7, W2 = 0.2, (c) W1 = 0.7, W2 = 0.3.

3.2.3.2. Modified Method of H-K Stacking. In this method, Tps is read from the receiver functions and H and Tppps is calculated for the values of K between 1.5 and 2.0 using Tps arrival time. The value of the receiver function at the predicted Tppps arrival time is drawn with the K value used to calculate that arrival time. The result should be a function with a peak at the appropriate K value.

This method works for one receiver function at a time. Normally, the stacked receiver function is used to calculate the K.

In this method, as in the previous one, the final selection is made using the stacked version of the receiver functions and much of the information buried in the individual receiver functions are lost. In fact both of these methods work best in the ideal situation where all peaks overlap perfectly and do not tolerate any spurious shifting about a mean value. However we know already that peaks of the receiver functions usually shifts in time due to variations of the incidence angle of arriving rays, complex geometry of the Moho interface, etc. (Zhu *et al.* 2006)

3.2.3.3. New Method by Window Stacking. In this study, the method above is improved by making it applicable to several receiver functions with slightly different Tppps times. The algorithm calculates the predicted arrival time as in the previous method but instead of plotting the value of the receiver function at that exact time, it searches for the maximum value of the receiver function in a certain time window. This method allows a tolerance for the spurious shifting of the peaks and therefore is expected to perform better in situations where the number of receiver functions is limited and therefore do not allow any corrections for geometric complexities. The resulting plot represents the K-H relationship for all of the receiver functions of a single station.

First a Tps has to be determined. It can either be determined by hand for each individual receiver function or by averaging the maxima of all of the receiver functions in a time window which has been determined by looking at all of the receiver functions. By inspecting the histogram of the arrival times of individual receiver functions which are the maximum of the receiver function in a given time window, whether or not this window has a common spike for all events can be decided.

In Zhu's method, after determining the Tps, the arrival time of the Ppps phase for different K are calculated and the amplitude of the stacked receiver function at that time is plotted.

In this method, the maximum amplitude in the neighborhood of calculated arrival time of Ppps phase of each Receiver Function is summed and plotted as in figure 3.6 in which different receiver functions from the same receiver are plotted

The multiples of discontinuities arrive at slightly different times because they cover a larger structure than Ps phases and suffer different velocity changes.

The advantage of this method is it does not suffer from slightly different arrival times of individual Receiver Functions which would disappear with stacking.

If there are two peaks in this graph, the one closer to the average is selected.

When calculating Tppps values for different K, the following formulas are used:

$$H=-Tps/(-(-(-K^2+p^2*Vp^2)/Vp^2)^(1/2)+(-(-1+p^2*Vp^2)/Vp^2)^(1/2)) \quad (3.6)$$

$$Tppps=H * (sqrt(K^2/Vp^2 - p^2) + sqrt(1/Vp^2 - p^2)) \quad (3.7)$$

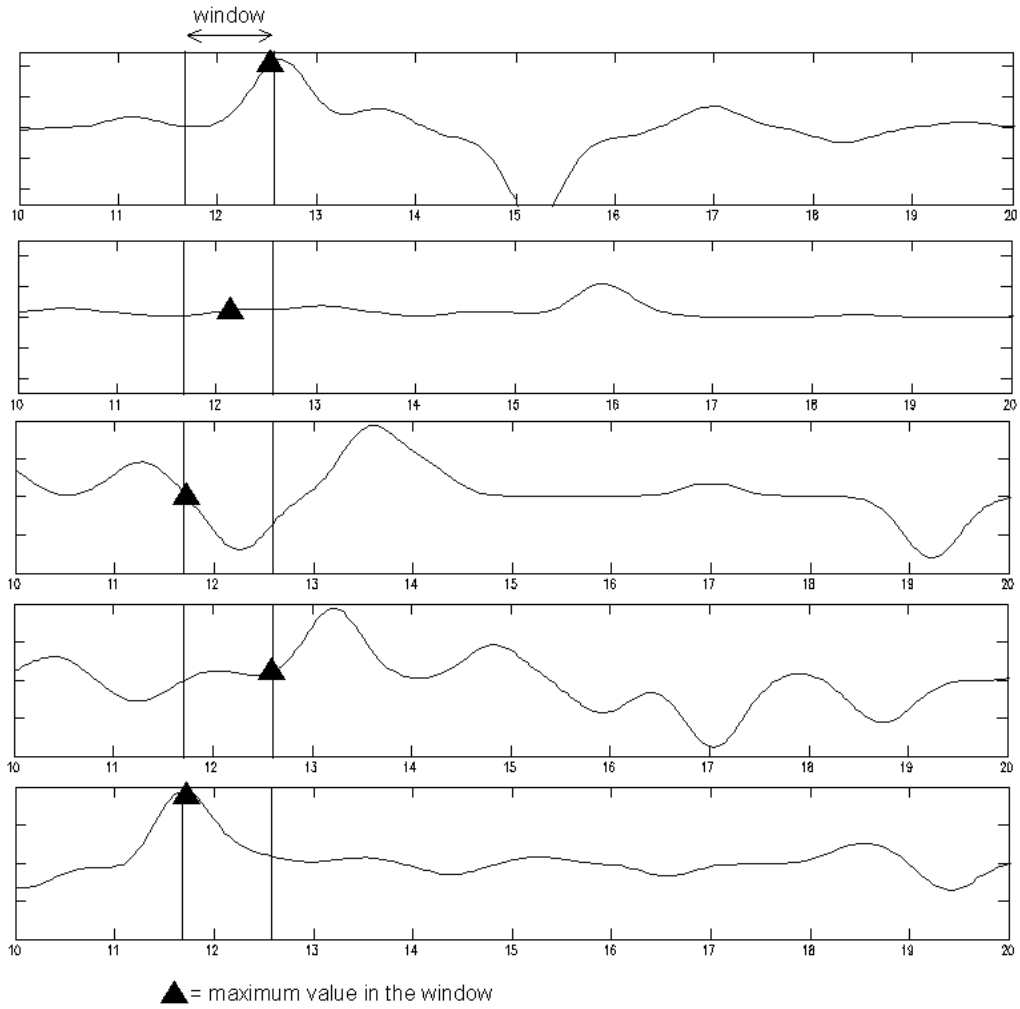

Figure 3.6. Demonstration of "window-stack method" used in this study. For determining the final amplitude in K vs. receiver function amplitude plot, the maximum value inside the designated window is selected.

3.2.4. Rotation

Rotation is necessary to isolate the P and converted S waves. Whether a 1-dimensional rotation is enough or 2-dimensional rotation is necessary depends on the distribution of the seismic events. In this study, most of the events come from epicenters which are 60 degrees away. To see the effect of rotating the waveforms around two axes the following experiment is made.

Sample waveforms of three components of station BLCB are rotated from 0 to 30 degrees. Then the receiver functions are calculated using the same algorithm which has been used to calculate the Receiver Functions throughout the rest of the study. The result

shows clearly that rotation of the waveforms around horizontal axis do not improve the results in any way noticable.

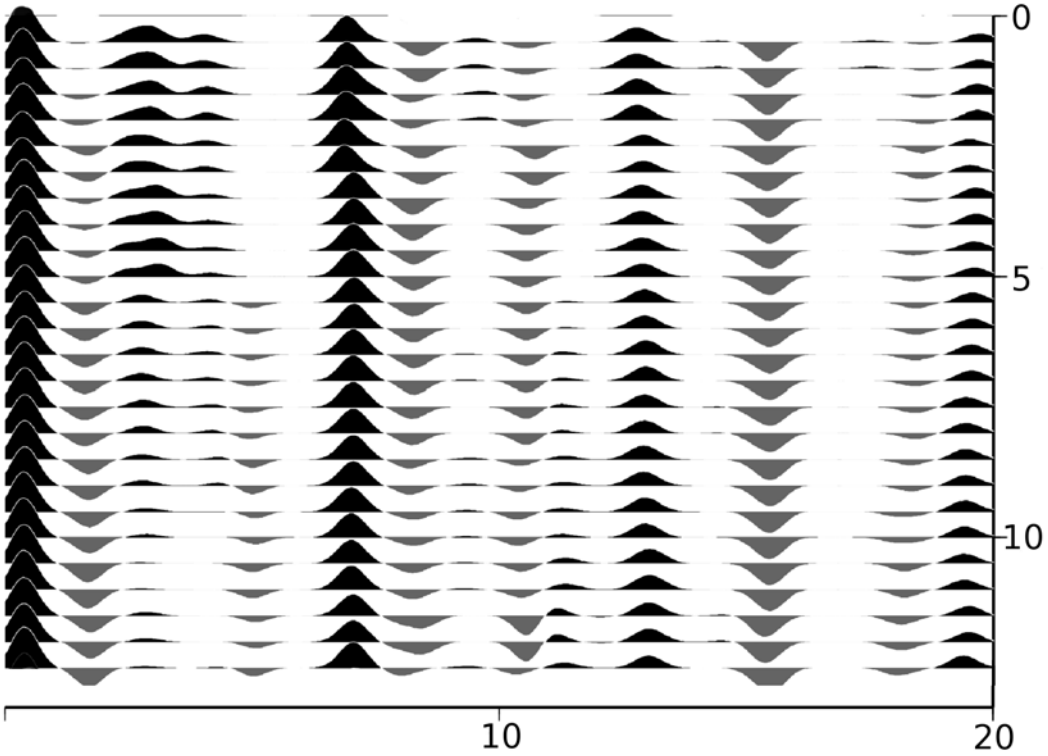

Figure 3.7. The result of the rotation experiment. Vertical axis indicates the rotation in degrees around T (SH) axis. The horizontal axis is time in seconds. No change is observed in the phase arriving around 0.5 seconds.

This conclusion was achieved with the following experiment. An event with average distance and back azimuth is selected. Then it is transformed from NWZ coordinate system to RTZ coordinate system. Then it is incrementally rotated by 0.5 degrees around T axis and receiver functions corresponding to each increment has been calculated.

The result, which shows no considerable difference between the receiver functions of first 15 degrees of rotation, can be seen in the figure below.

After this experiment, it has been decided that rotation to RTZ coordinate system is enough for this study.

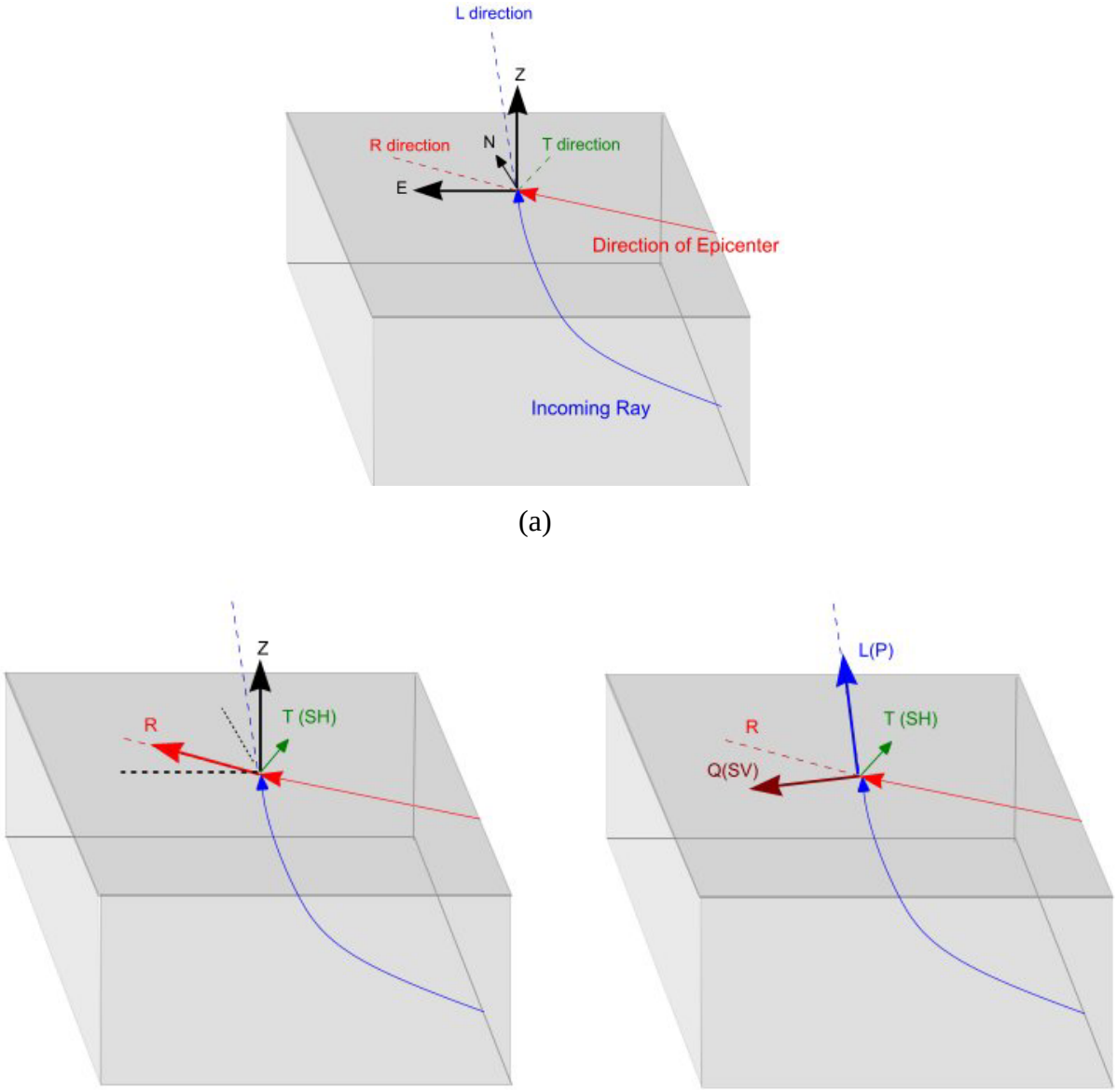

Figure 3.8. The illustration of rotation of coordinate systems for incoming events. (a) is the state of no rotation. (b) is the state of rotation to RTZ coordinate system, which is used throughout this study. (c) is the state to QLT coordinate system which is very close to the RTZ system for distant events.

4. DATA AND RESULTS

The data consists of waveforms collected from 8 online and 4 offline broadband seismic stations in the southwestern Anatolia between April 2006 and July 2007. Event list which is downloaded from USGS website consisted of 350 events which were 30 to 95 degrees away of which the distribution according to their back azimuth and distance are given in Figure 4.1 and geographic locations are given in Figure 4.2. The lower magnitude limit of the events was 5.5.

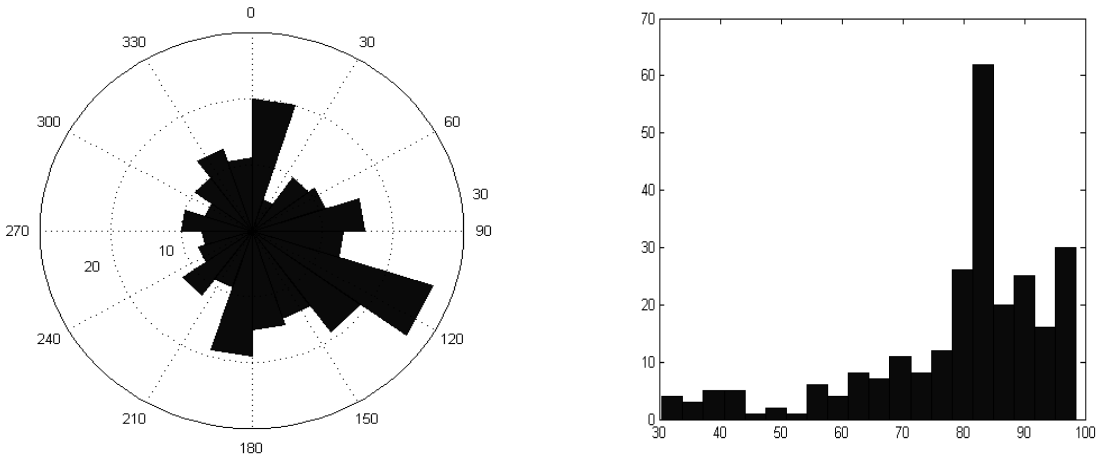

(a) (b)

Figure 4.1. The distribution of events according to their (a) back azimuth, (b) distance in degrees.

Figure 4.2. The distribution of the events which took place between 04.01.2006 and 07.31.2007.

P wave arrival times were calculated using a program called ttim which uses IASP91 tables to calculate arrival times of events. Since exact time of P wave arrival is not necessary, picking of P-wave arrival is completely automatized.

Butterworth bandpass filter is applied to the observed seismograms for corner periods of 0.1 and 2.0 Seconds. The waveforms then are cut 60 seconds before and 90 seconds after the calculated P arrival. Then XYZ components are transformed into RTZ coordinate system.

Using algorithm of Ligoria and Ammon (1999), the receiver functions are calculated with 100 iterations and a Gaussian width factor of 2.5.

Bad receiver functions are then eliminated by hand. After the elimination, they are processed for calculating the H and K.

For calculation of H and K values, velocity of P waves, *Vp* is assumed to be 6.2 km/s, ray parameter p, 0.06.

Most of the stations are located near Gökova Bay (Figure 4.3) except BLCB and ELL which lie due to the north and east of the bay respectively.

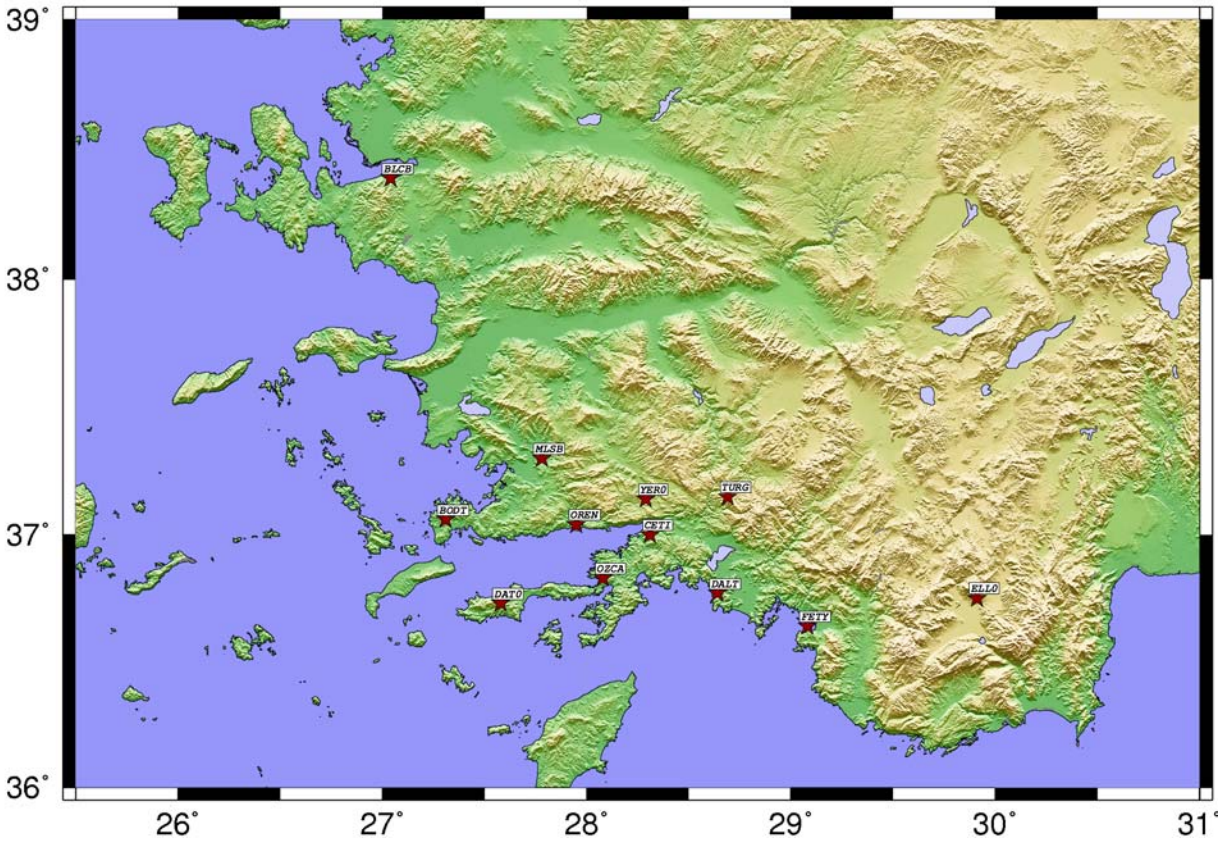

Figure 4.3. The distribution of seismic stations on the map.

4.1. Data Availability

Data was collected during a period of 15 months. The distribution of the data is given in the Figure 4.4. In offline stations TURG and OZCA, data collection begins in November of 2006. In online stations, data are present since April 2004. There are some gaps in the data as seen below. As a result, the events which are used to calculate receiver functions are not exactly the same for each station.

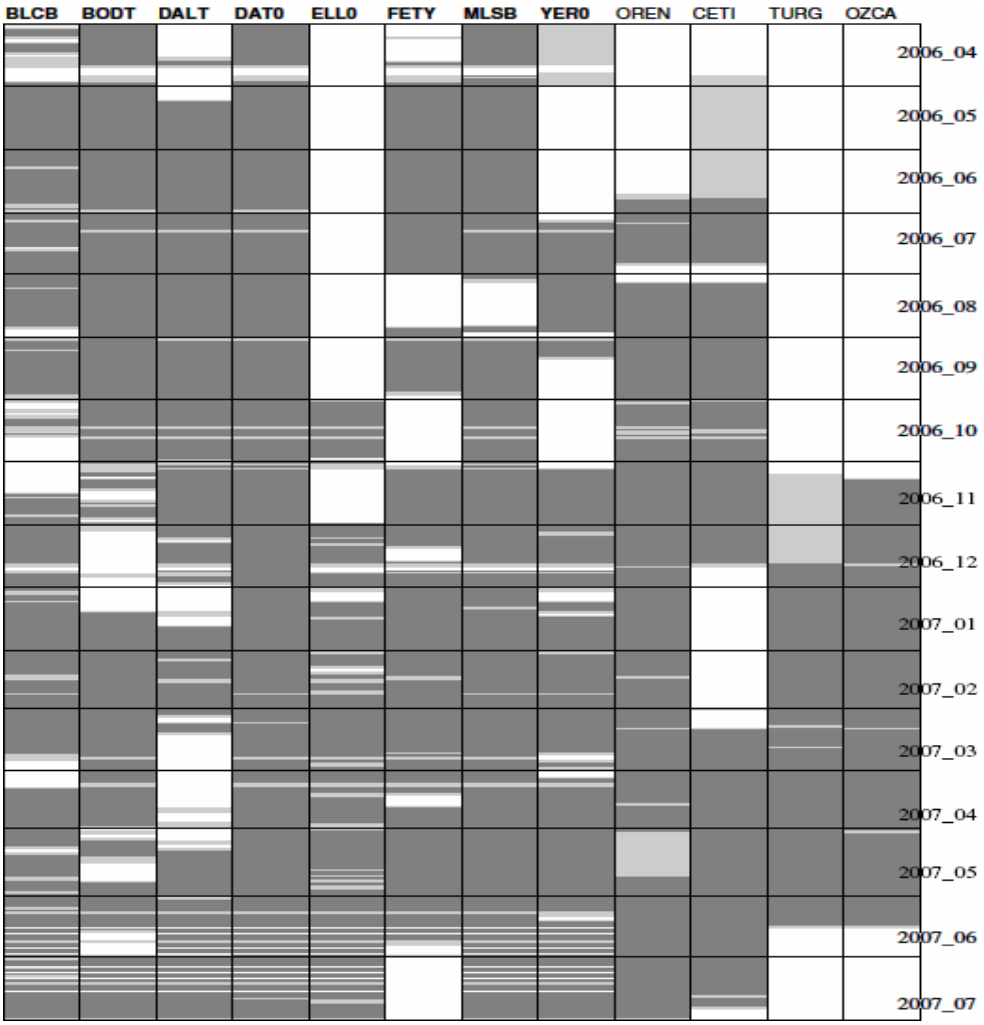

Figure 4.4. Chart indicating the available data in stations during data collection period. The vertical axis is time. Dark grey areas indicate complete data whereas light grey and white areas indicate incomplete and missing data respectively.

4.2. Results by Stations

4.2.1. Station BLCB

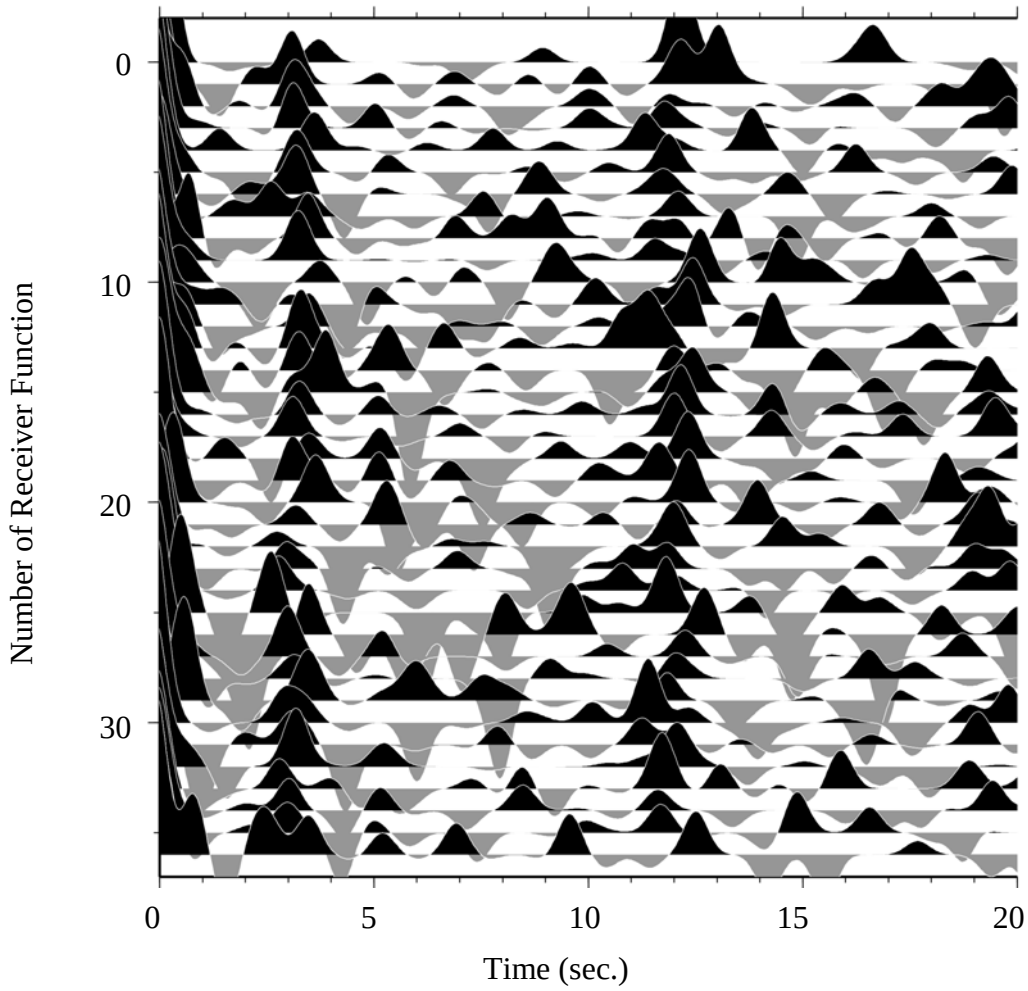

Figure 4.5. Receiver functions of BLCB.

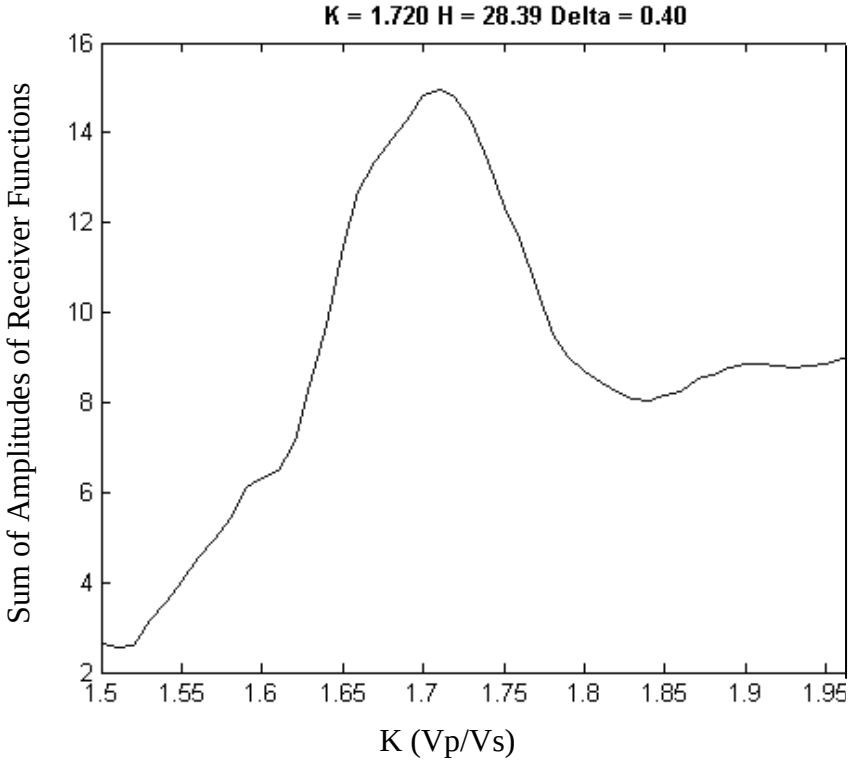

Figure 4.6. Kappa vs. amplitude plot of BLCB calculated with a window of 0.4 seconds.

There were a total of 222 events which were in the appropriate back azimuth and distance range.

A phase can be noticed (Figure 4.5) which is probably primary moho conversion at 3.4 seconds. Another low amplitude phase can be noted at 5 seconds which is followed by a negative low amplitude phase. The moho multiple can be seen at 12 seconds.

The station is located in the southern side of the Gökova Bay. It is a permanent station on solid bedrock. As a result the receiver functions are relatively clear.

This station yields a Kappa of 1.720 and thickness of 28.39 km. (Figure 4.6).

4.2.2. Station BODT

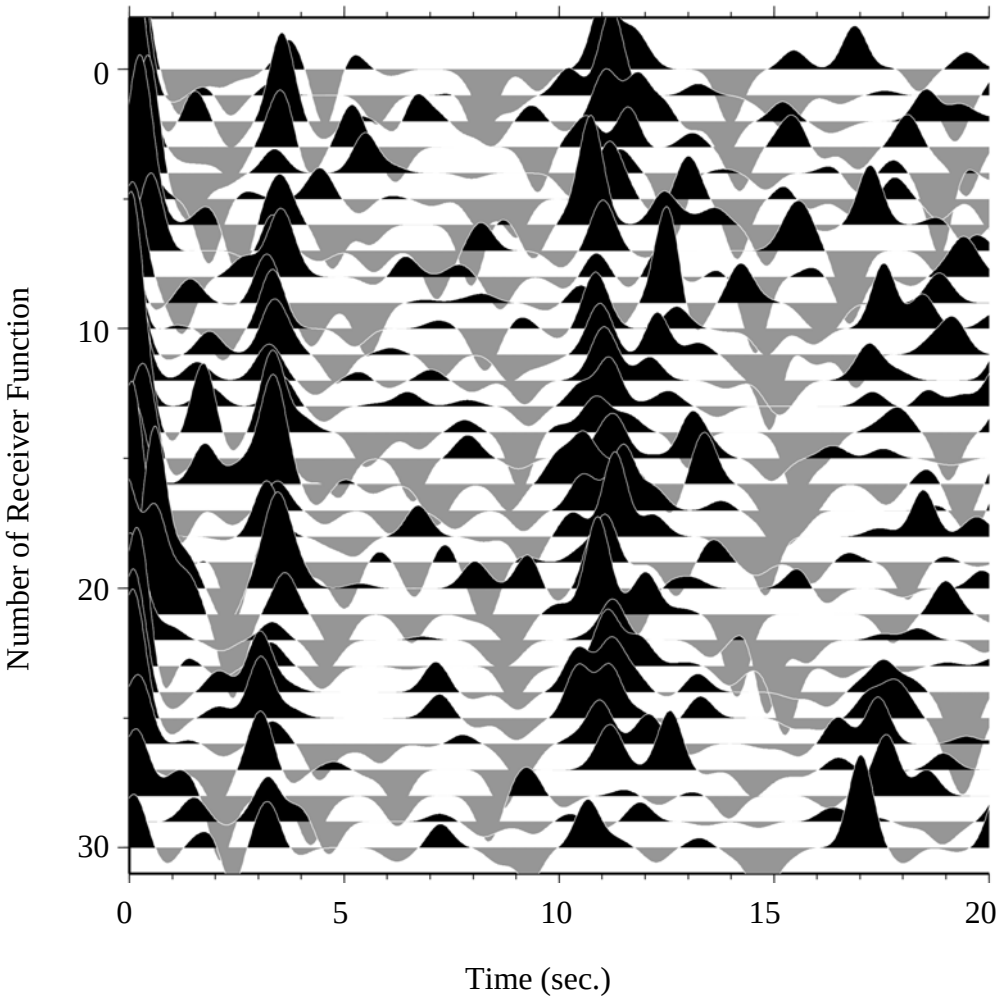

Figure 4.7. Receiver functions of BODT.

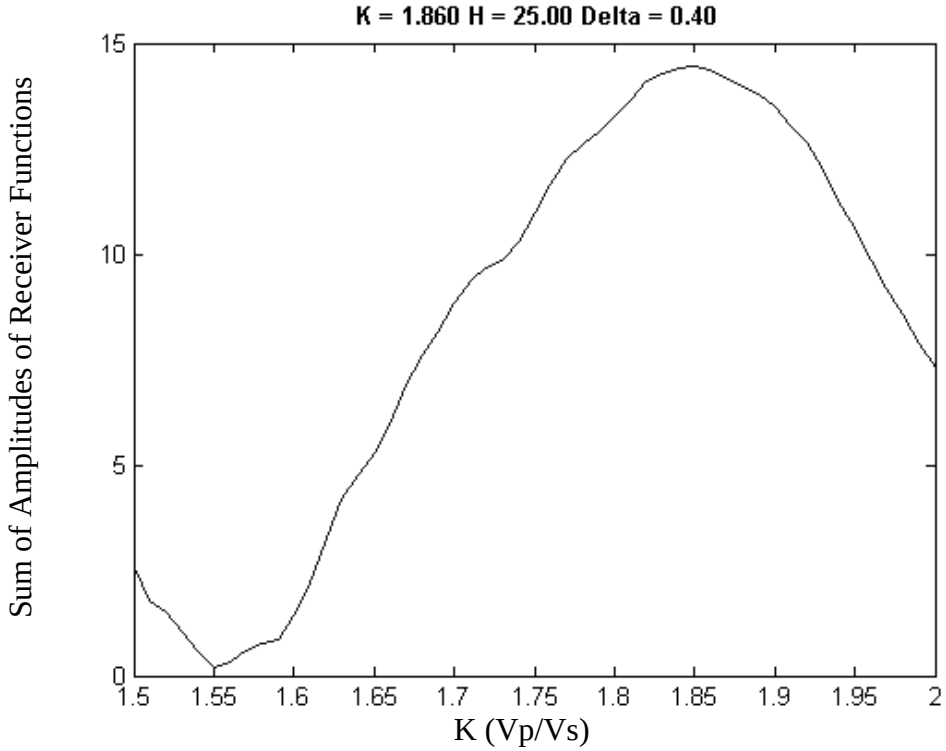

Figure 4.8. Kappa vs. amplitude plot of BODT calculated with a window of 0.4 seconds.

The low threshold for the magnitude of events in this station is 5.5. There were a total of 167 events which were in the appropriate back azimuth and distance range.

A phase can be noticed (Figure 4.7) which is probably primary Moho conversion at 3.6 seconds. The Moho multiple can be seen at 12 seconds well enough.

The station is located on the northern side of Gökova bay. It is a permanent station on solid bedrock. As a result the receiver functions are relatively clear.

This station yields a Kappa of 1.860 and thickness of 25.00 km. (Figure 4.8).

4.2.3. Station CETI

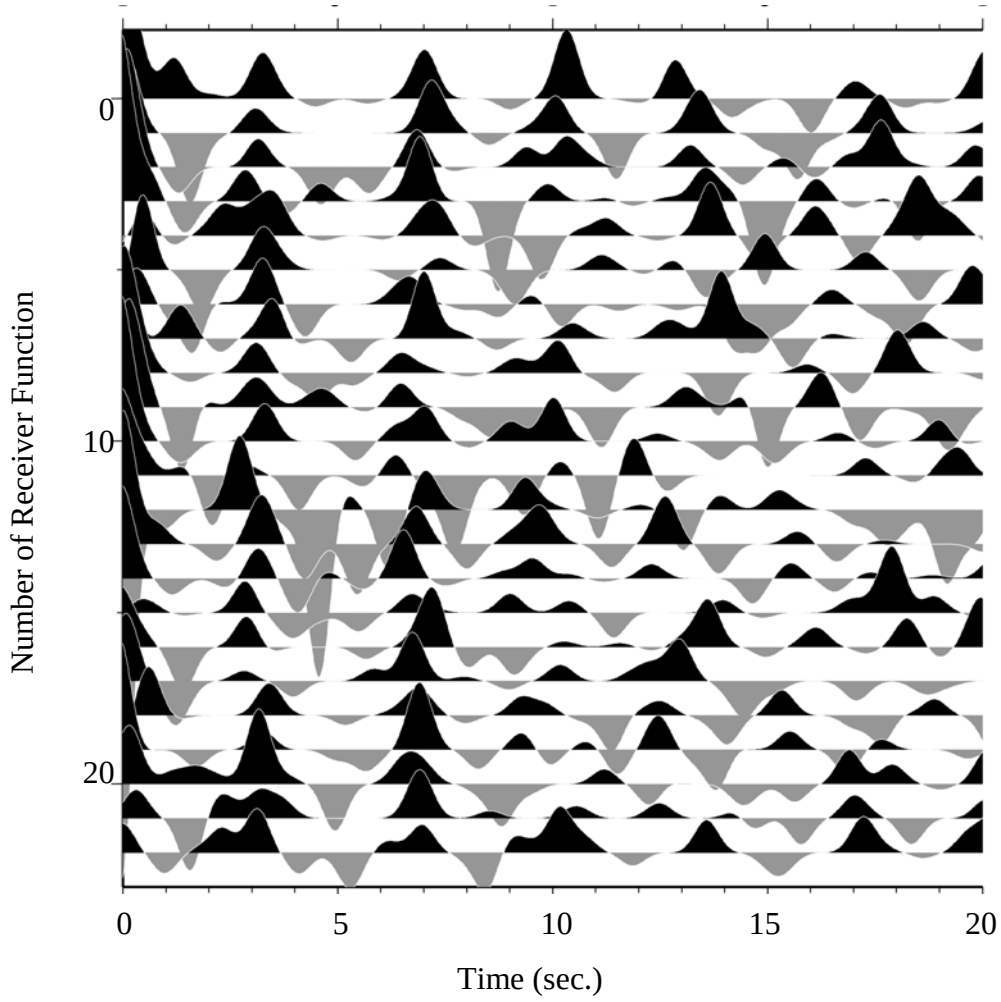

Figure 4.9. Receiver functions of CETI.

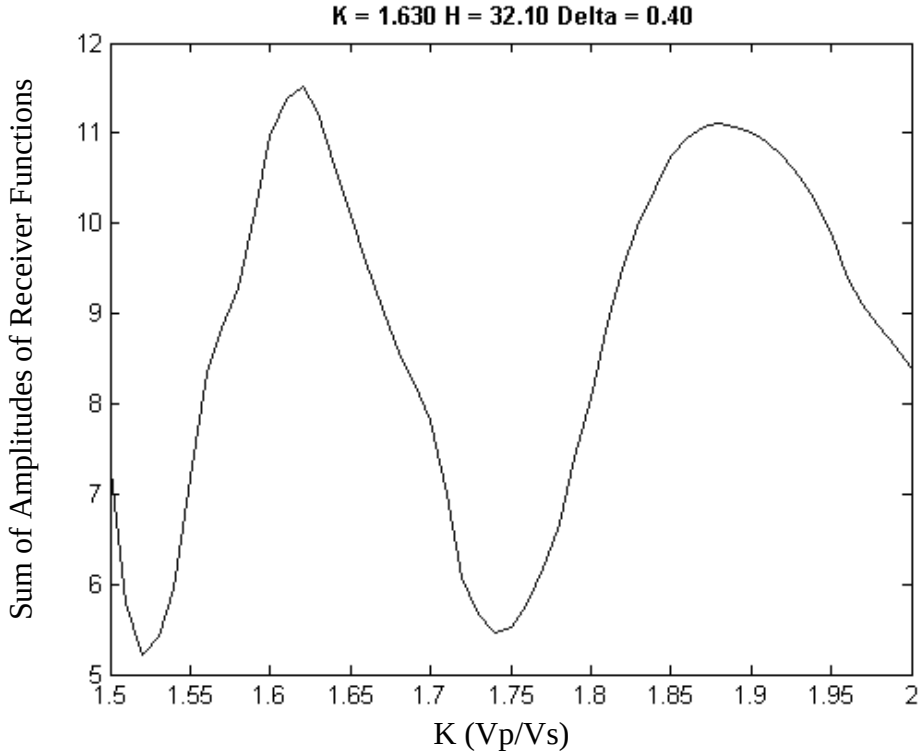

Figure 4.10. Kappa vs. amplitude plot of CETI calculated with a window of 0.4 seconds.

The low threshold for the magnitude of events in this station is 5.5. There were a total of 121 events which were in the appropriate back azimuth and distance range.

A phase can be noticed (Figure 4.9) which is probably primary moho conversion at 3.4 seconds. Another phase can be noticed at 6.6 seconds. The moho multiple can be seen at 12 seconds well enough. The K vs amplitude graph has two peaks. Second peak is closer to the average value of the K and it is used to calculate the H for this station.

The station is located at the end of Gökova bay. It is an offline station on solid bedrock. The receiver functions are less noisy than those of online stations but still relatively good.

This station yields a Kappa of 1.630 and thickness of 32.10 km. (Figure 4.10).

4.2.4. Station DALT

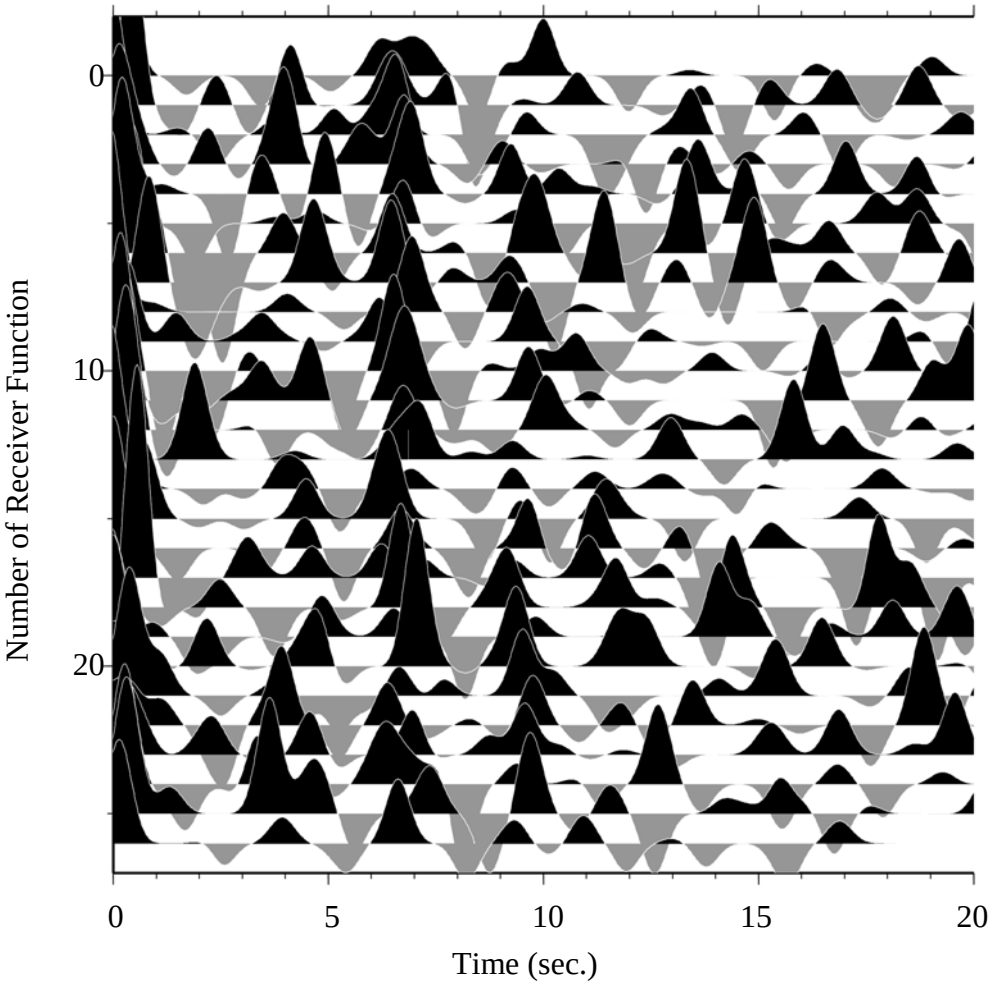

Figure 4.11. Receiver functions of DALT.

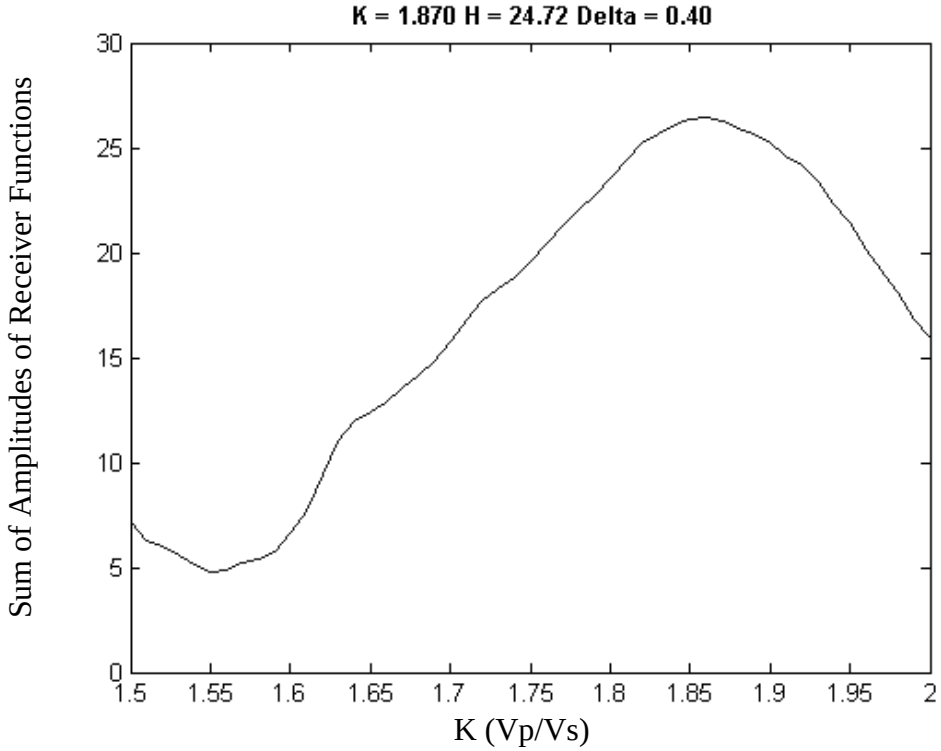

Figure 4.12. Kappa vs. amplitude plot of DALT calculated with a window of 0.4 seconds.

The low threshold for the magnitude of events in this station is 5.5. There were a total of 167 events which were in the appropriate back azimuth and distance range.

There are no clear conversion phases which could be interpreted as Moho (Figure 4.11). However two conversion phases can be seen at 6.8 and 9.6 seconds.

Altough the K-amplitude graph has one clear peak at (K=1.870) it can not be interpreted as a solution. (Figure 4.12).

It is a permanent station.

4.2.5. Station DAT

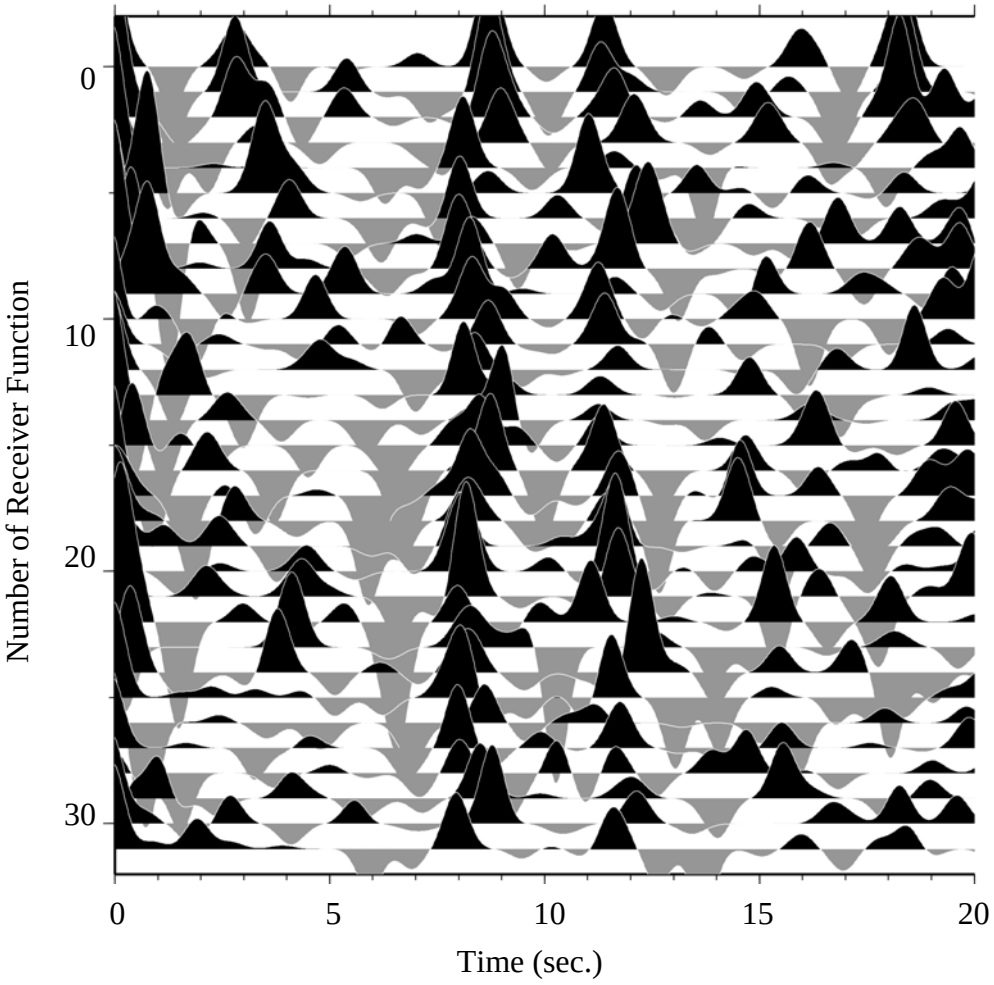

Figure 4.13. Receiver functions of DAT.

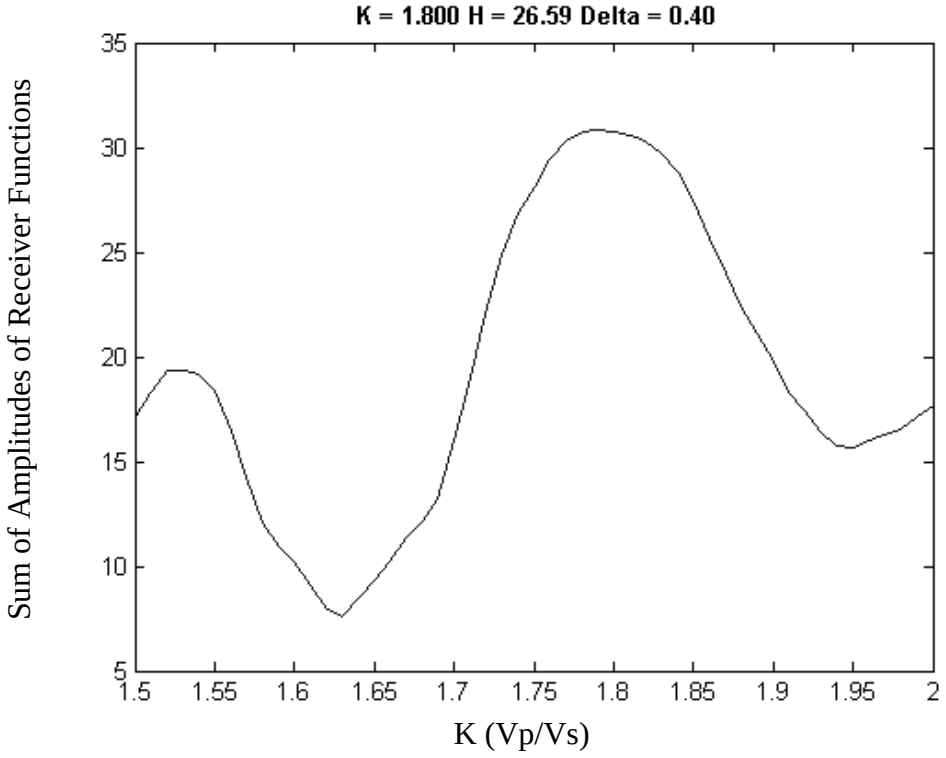

Figure 4.14. Kappa vs. amplitude plot of DAT calculated with a window of 0.4 seconds.

The low threshold for the magnitude of events in this station is 5.5. There were a total of 256 events which were in the appropriate back azimuth and distance range.

There are no clear conversion phases (Figure 4.13) which could be interpreted as moho. However a clear conversion can be seen at 8.5 seconds. Altough no moho conversion phases are observed, there is a positive phase at 12 seconds which is at about the same time as a moho multiple.

The station is located in the southern side of the Gökova Bay. It is a permanent station on solid bedrock. As a result the receiver functions are relatively clear.

This station yields a Kappa of 1.800 and thickness of 26.59 km. (Figure 4.14).

4.2.6. Station ELL

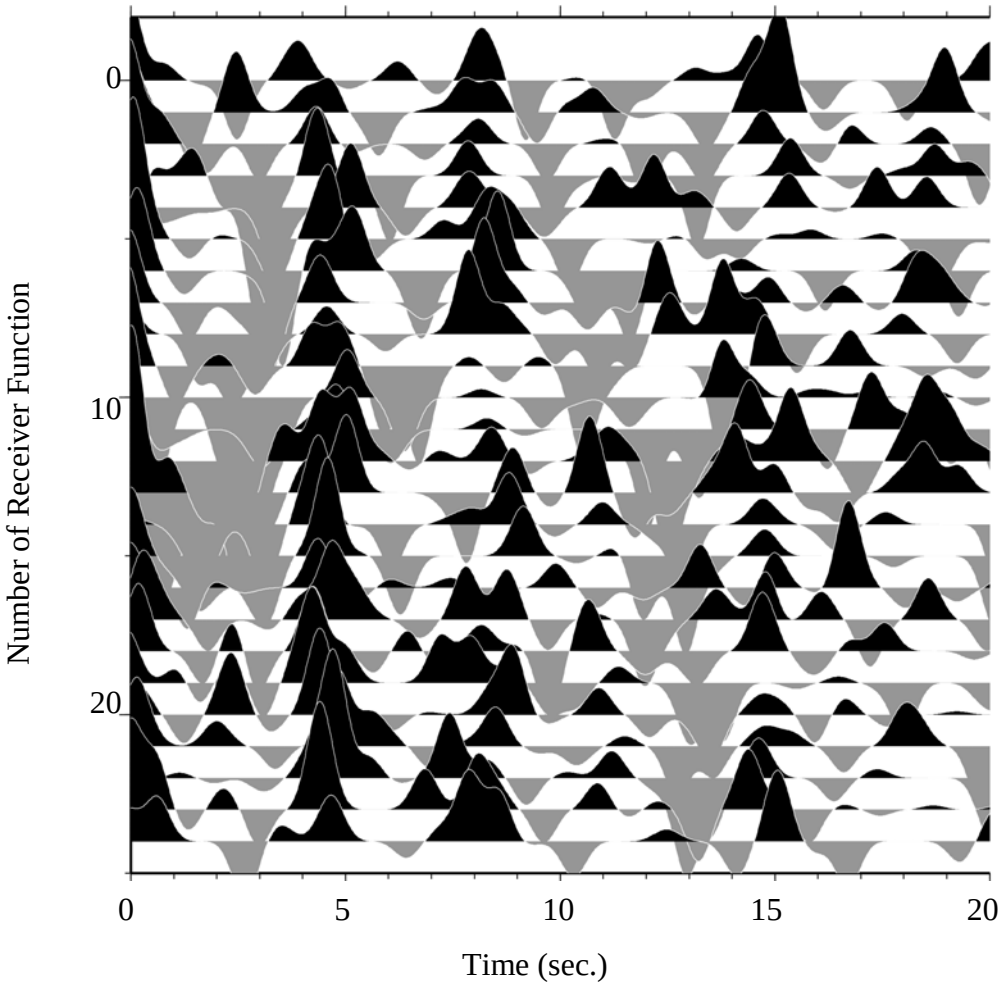

Figure 4.15. Receiver functions of ELL.

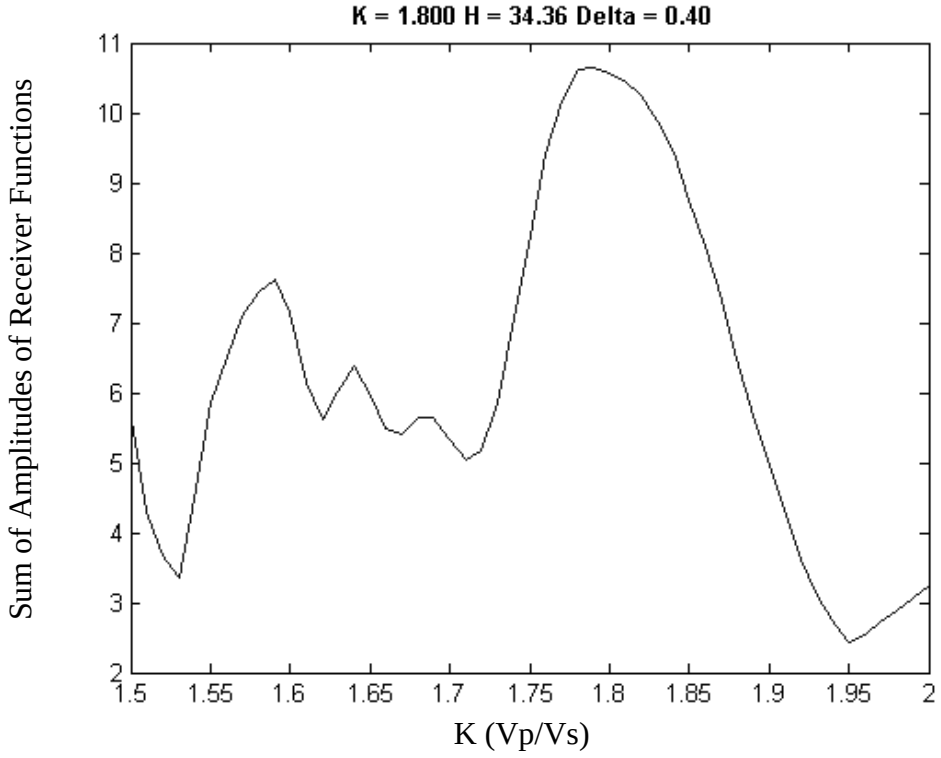

Figure 4.16. Kappa vs. amplitude plot of ELL calculated with a window of 0.4 seconds.

The low threshold for the magnitude of events in this station is 5.5. There were a total of 78 events which were in the appropriate back azimuth and distance range.

The Moho conversion phase (Figure 4.15) arrives at 4.6 seconds, which indicates a thick crust, as expected in the region. Another phase arrives at 7.7 seconds which is quite coherent throughout the receiver functions. It might indicate a second crustal Moho beneath Anatolian Moho.

This station yields a Kappa of 1.800 and thickness of 34.36 km. (Figure 4.16).

4.2.7. Station FETY

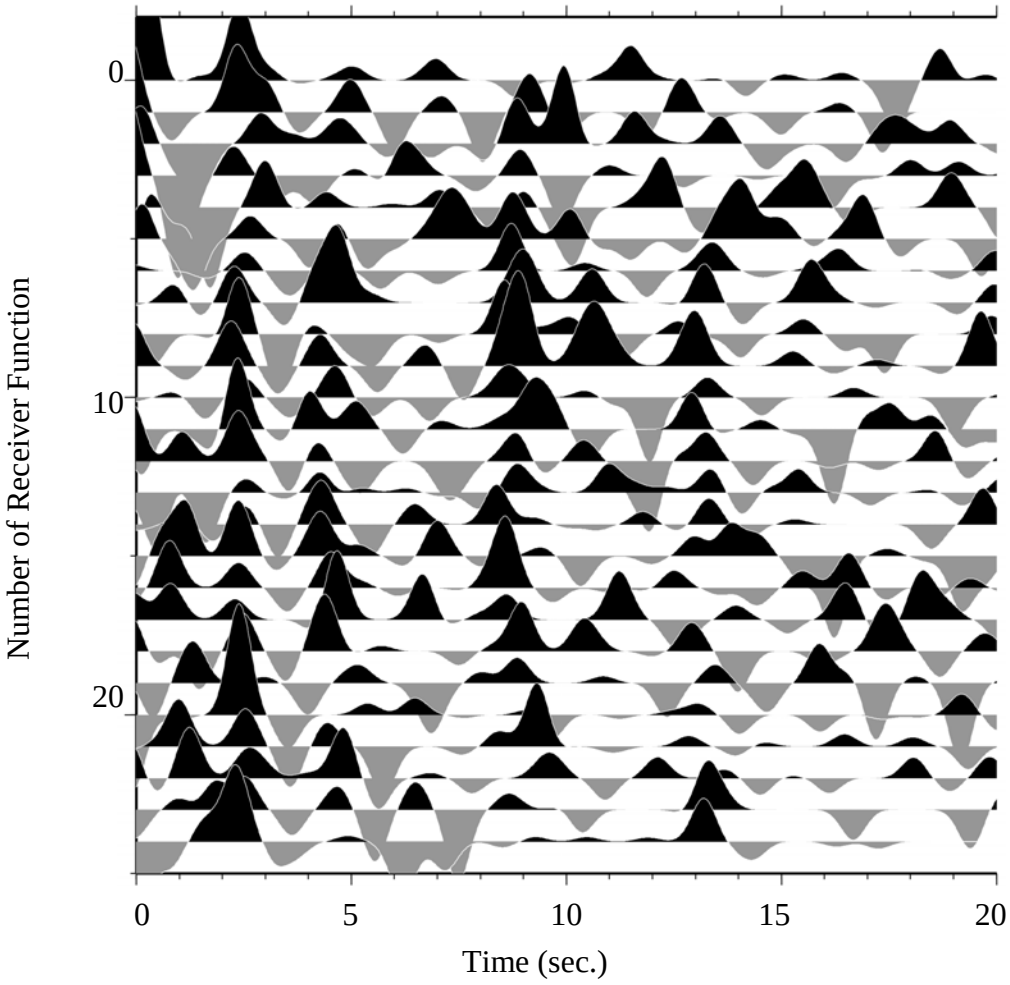

Figure 4.17. Receiver functions of FETY.

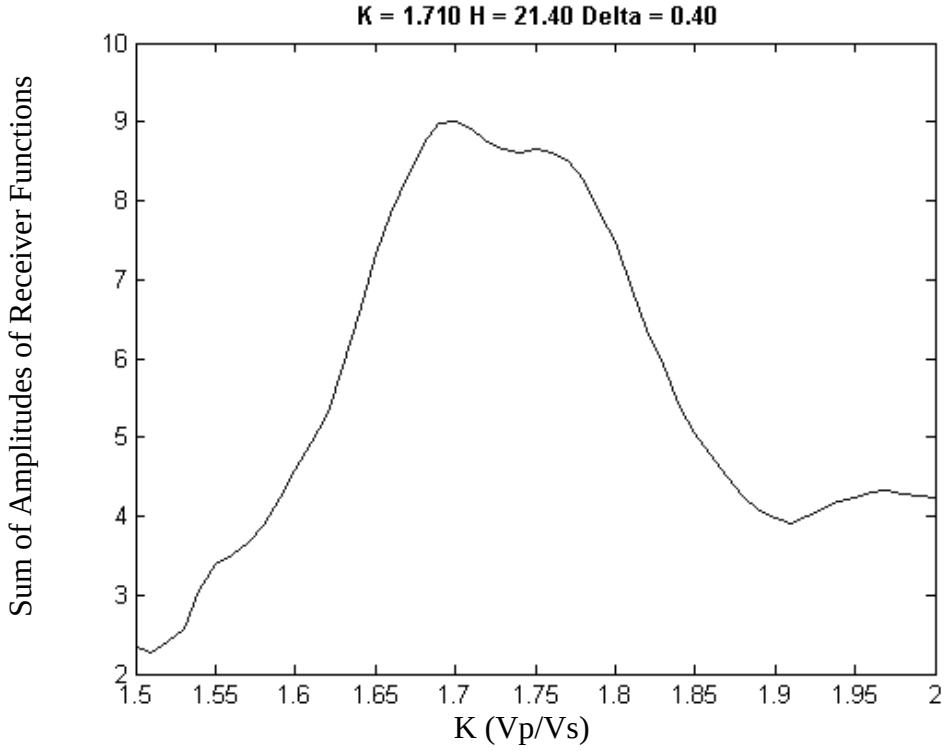

Figure 4.18. Kappa vs. amplitude plot of FETY calculated with a window of 0.4 seconds.

The low threshold for the magnitude of events in this station is 5.5. There were a total of 61 events which were in the appropriate back azimuth and distance range.

There is a conversion phase (Figure 4.17) at 2.6 seconds which can be interpreted as Moho. The multiple of the Moho conversion is at 8.9 seconds. Another phase can be seen at 14 seconds.

It is a permanent station 50 km.s south of Gökova Bay.

This station yields a Kappa of 1.710 and thickness of 21.40 km. (Figure 4.18).

4.2.8. Station MLSB

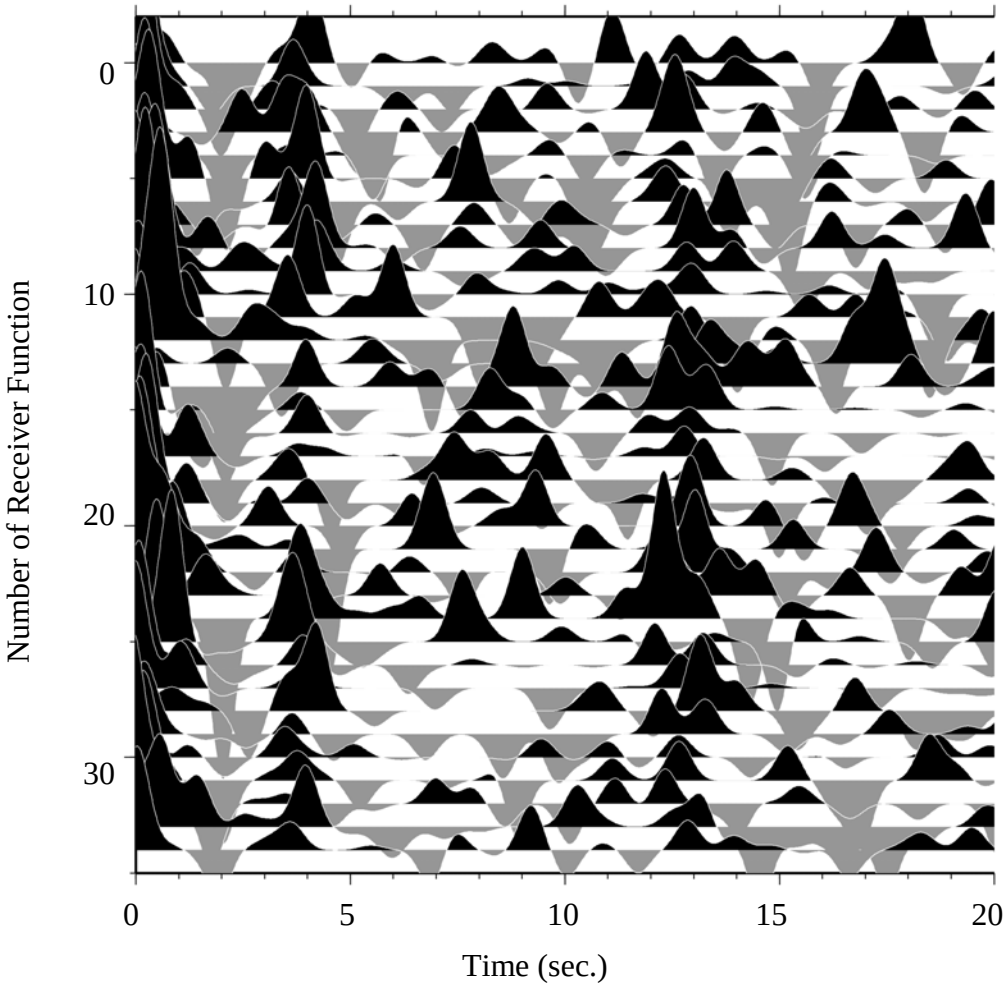

Figure 4.19. Receiver functions of MLSB.

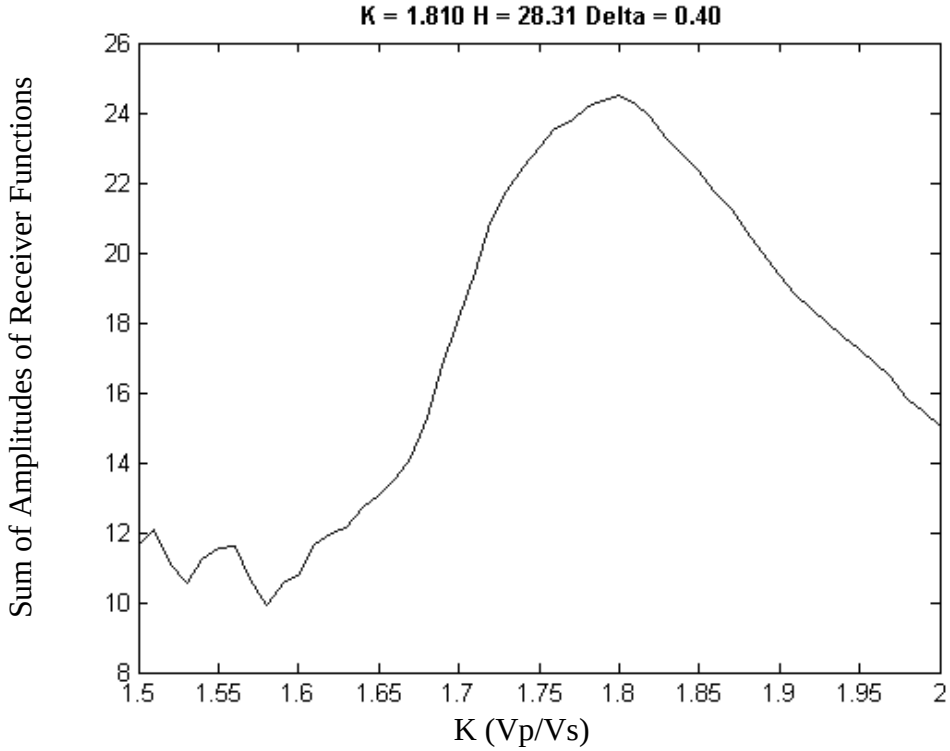

Figure 4.20. Kappa vs. amplitude plot of MLSB calculated with a window of 0.4 seconds.

The low threshold for the magnitude of events in this station is 5.5. There were a total of 196 events which were in the appropriate back azimuth and distance range.

A phase can be noticed (Figure 4.19) which is probably primary moho conversion at 3.8 seconds. The moho multiple can be seen at 13 seconds well enough.

The station is located on the 50 kms north of Gökova Bay. It is a permanent station on solid bedrock. As a result the receiver functions are relatively clear.

This station yields a Kappa of 1.810 and thickness of 28.31 km. (Figure 4.20)

4.2.9. Station TURG

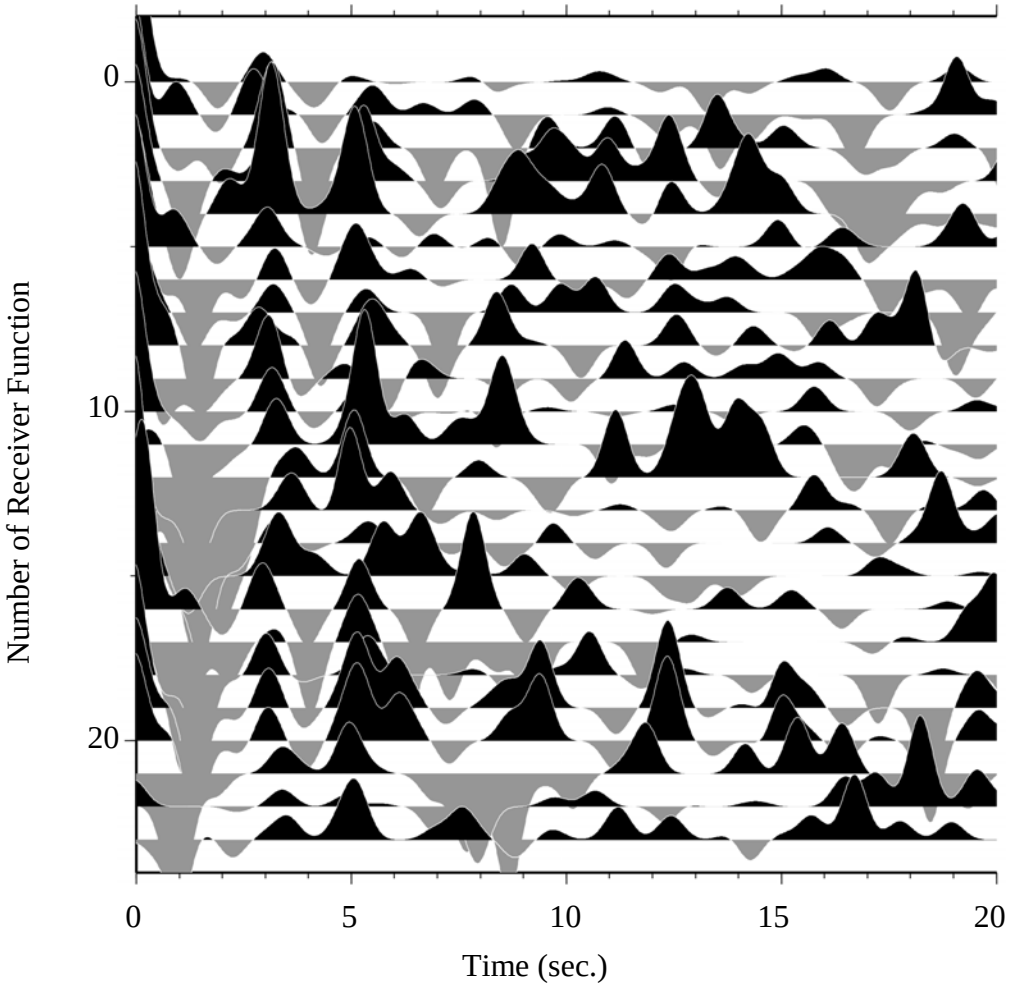

Figure 4.21. Receiver functions of TURG.

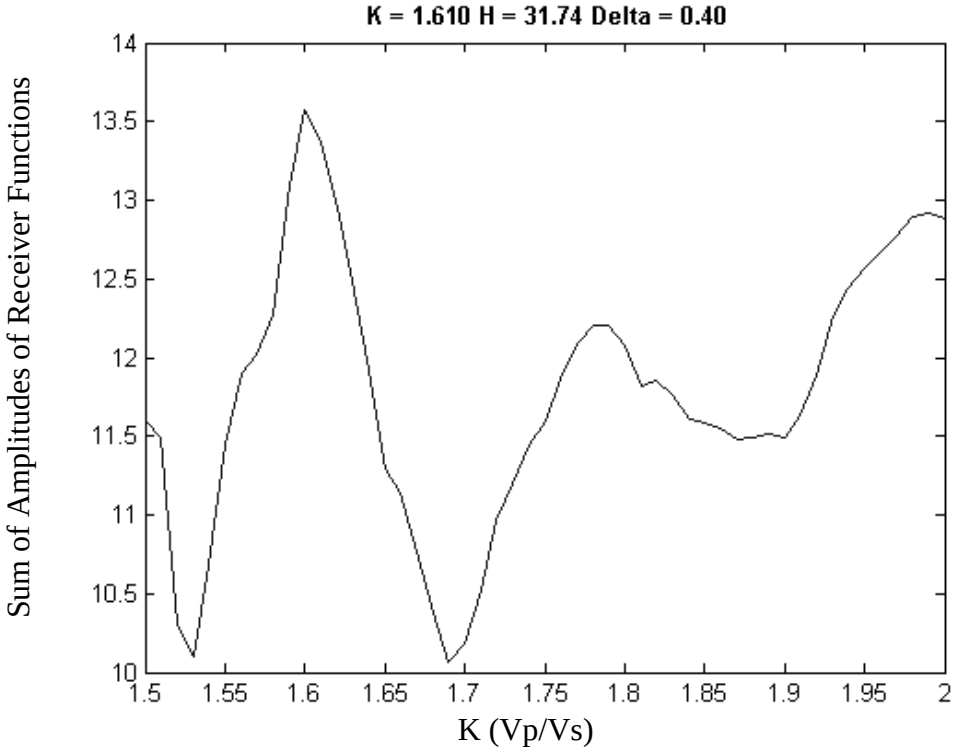

Figure 4.22. Kappa vs. amplitude plot of TURG calculated with a window of 0.4 seconds.

The low threshold for the magnitude of events in this station is 5.5. There were a total of 115 events which were in the appropriate back azimuth and distance range.

A phase can be noticed (Figure 4.21) which is probably primary moho conversion at 3.2 seconds. The multiple of this phase which should be around 12 seconds iowever is not very clear.

There is another phase at 5.3 seconds which is even more clear than moho conversion.

The station is located on the 50 km.s east of Gökova Bay. This is an offline station in a quiet location on solid bedrock.

This station yields a Kappa of 1.610 and thickness of 31.74 km. (Figure 4.22).

4.2.10. Station OREN

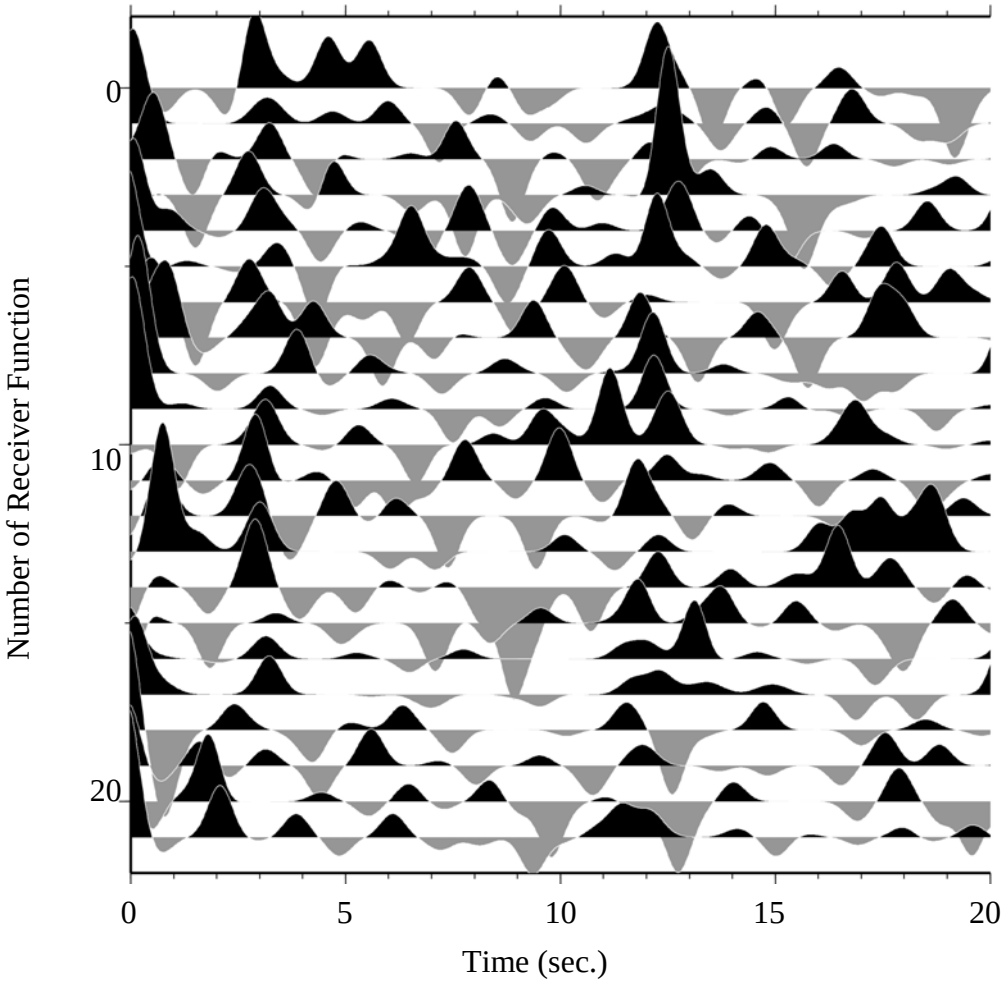

Figure 4.23. Receiver functions of OREN.

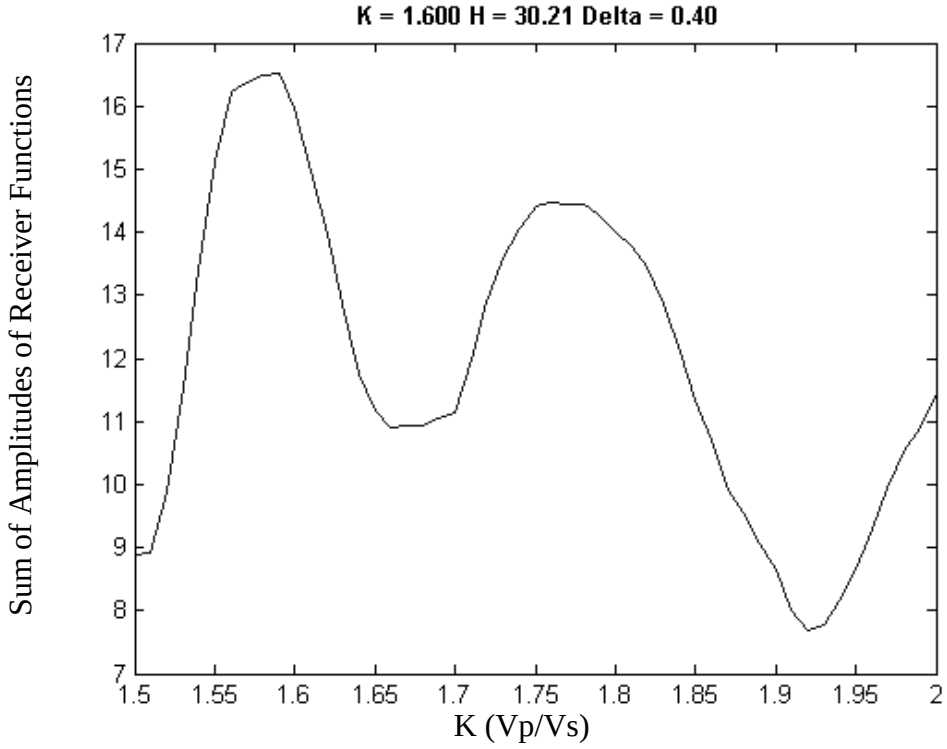

Figure 4.24. Kappa vs. amplitude plot of OREN calculated with a window of 0.4 seconds.

The low threshold for the magnitude of events in this station is 5.5. There were a total of 186 events which were in the appropriate back azimuth and distance range.

A phase can be noticed (Figure 4.23) which is probably primary moho conversion at 3.1 seconds. The multiple of this phase can be seen around 12 seconds.

The station is located on the northern coast of Gökova Bay. This is an offline station.

This station yields a Kappa of 1.600 and thickness of 30.21 km. (Figure 4.24).

4.2.11. Station OZCA

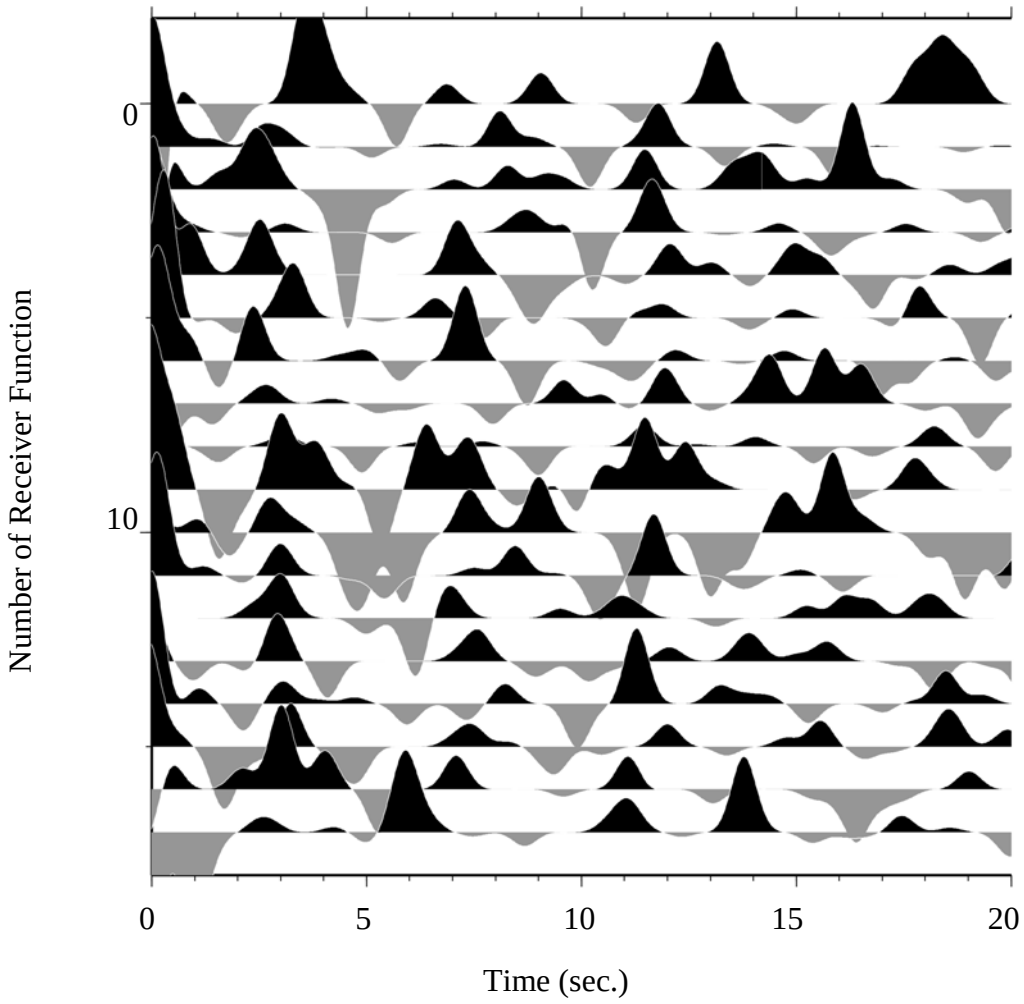

Figure 4.25. Receiver functions of OZCA.

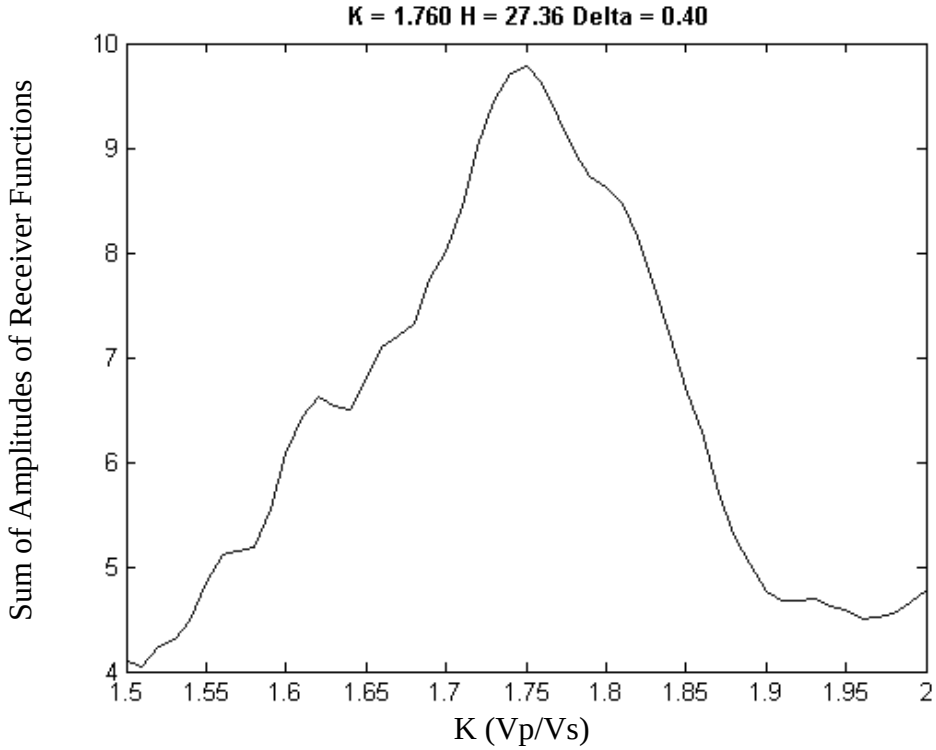

Figure 4.26. Kappa vs. amplitude plot of OZCA calculated with a window of 0.4 seconds.

The low threshold for the magnitude of events in this station is 5.5. There were a total of 141 events which were in the appropriate back azimuth and distance range.

There is a phase (Figure 4.25) which is probably primary Moho conversion at 3.5 seconds. The multiple of this phase can be seen around 12 seconds but it is not very clear.

There is another phase at 7.5 seconds.

The station is located eastern coast of Gökova Bay. This is an offline station.

This station yields a Kappa of 1.760 and thickness of 27.36 km. (Figure 4.26).

4.2.12. Station YER

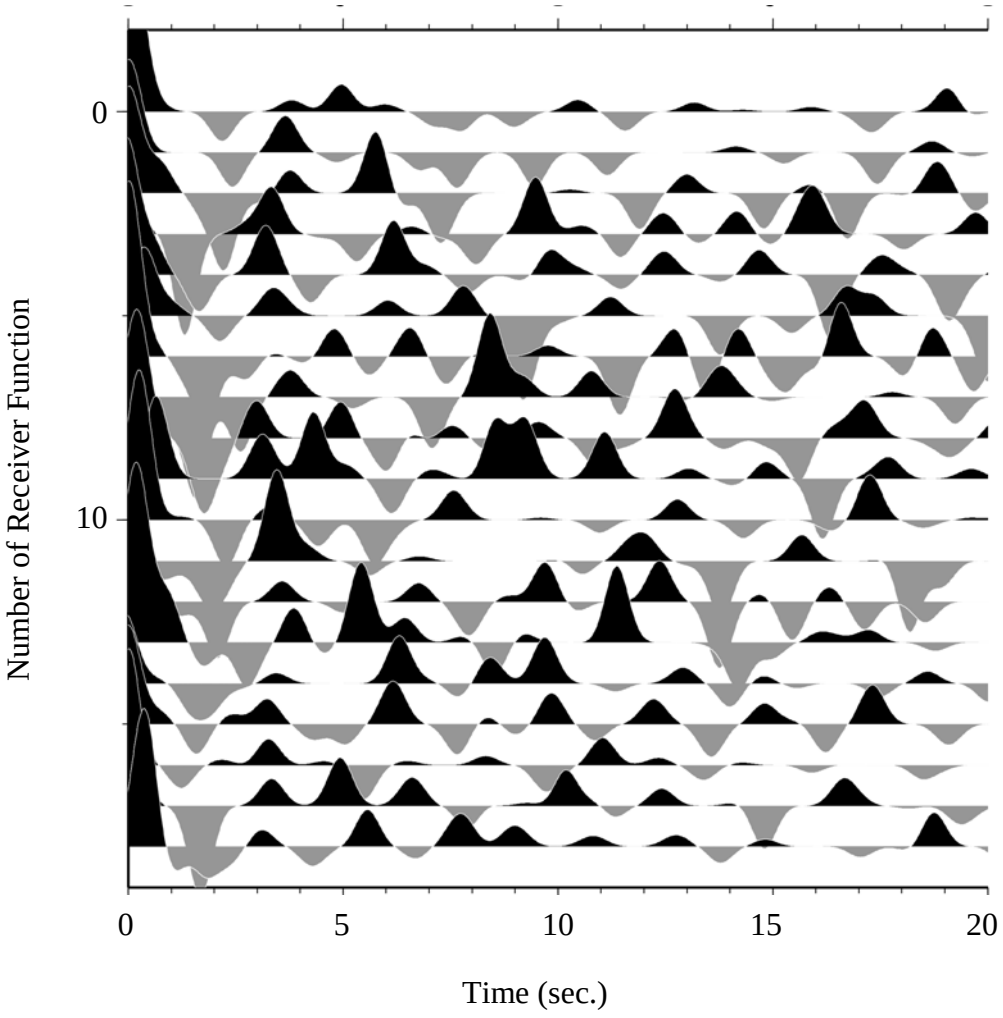

Figure 4.27. Receiver functions of YER.

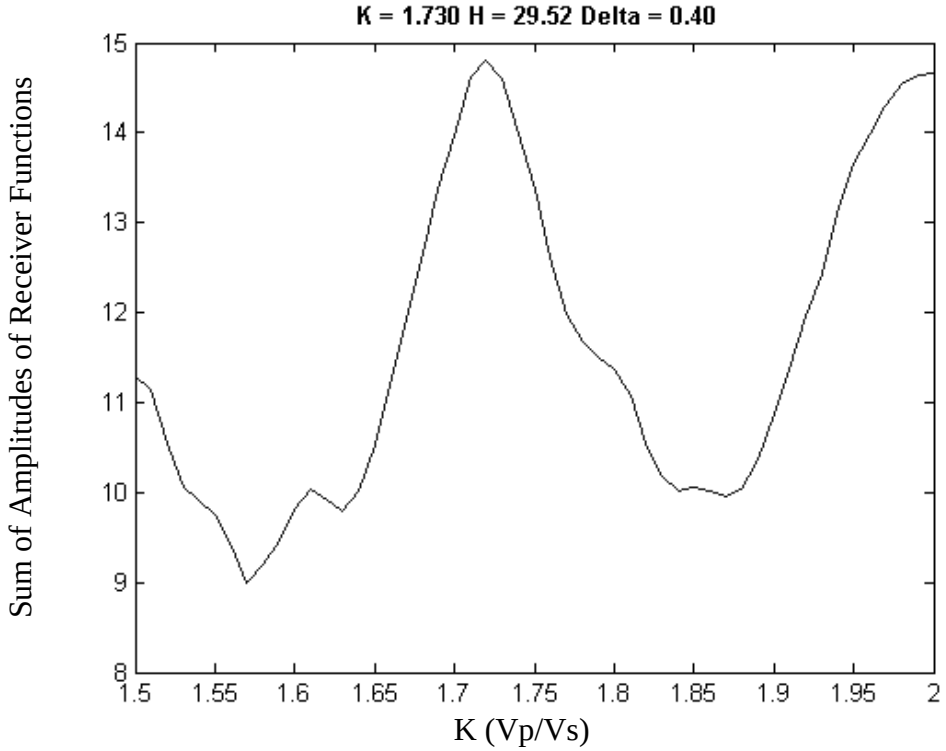

Figure 4.28. Kappa vs. amplitude plot of YER calculated with a window of 0.4 seconds.

The low threshold for the magnitude of events in this station is 5.5. There were a total of 189 events which were in the appropriate back azimuth and distance range.

A vague phase can be noticed which is probably primary Moho conversion at 3.6 seconds. The multiple of this phase also unclear and can be seen around 12.5 seconds.

The station is located on the northern side of Gökova Bay. This is an offline station.

This station yields a Kappa of 1.730 and thickness of 29.52 km. (Figure 4.28).

4.3. Summary of Results

Table 4.1 shows the delay time and the optimal choice of Kappa that produces the best fitting multiple (PPPs) for each station. Then a generic Kappa is found by averaging all the estimated ones, which give K=1.78. The remaining parameters are estimated using this generic value for Kappa. The depth of the Moho which corresponds to the optimal Kappa is also given together with the theoretical delay time for the multiple.

A contour map is shown in Figure 4.29 to illustrate the variation of the Moho topography across the study area. The Moho depths were fitted by adjustable tension continuous curvature surface gridding algorithm in GMT package (Wessel and Smith, 1998).

Table 4.1. The Moho depths calculated in stations where primary Tps phase (Aegean Moho) can be observed.

	K	**H**	**Tps**	**Tppps(K=Kmean)**
BLCB	1.72	28.39 ± 1.3460	3.4394	11.315
BODT	1.87	25.00 ± 1.9810	3.6054	11.861
CETI	1.88	23.12 ± 2.0472	3.4111	11.222
ELL0	1.80	34.36 ± 2.2708	4.6154	15.184
FETY	1.71	21.40 ± 1.1560	2.5566	8.4107
MLSB	1.81	28.31 ± 2.3694	3.8499	12.665
OREN	1.77	23.64 ± 1.6785	3.0596	10.065
TURG	1.79	24.62 ± 1.8717	3.2674	10.749
YER0	1.73	29.52 ± 1.9759	3.6243	11.923

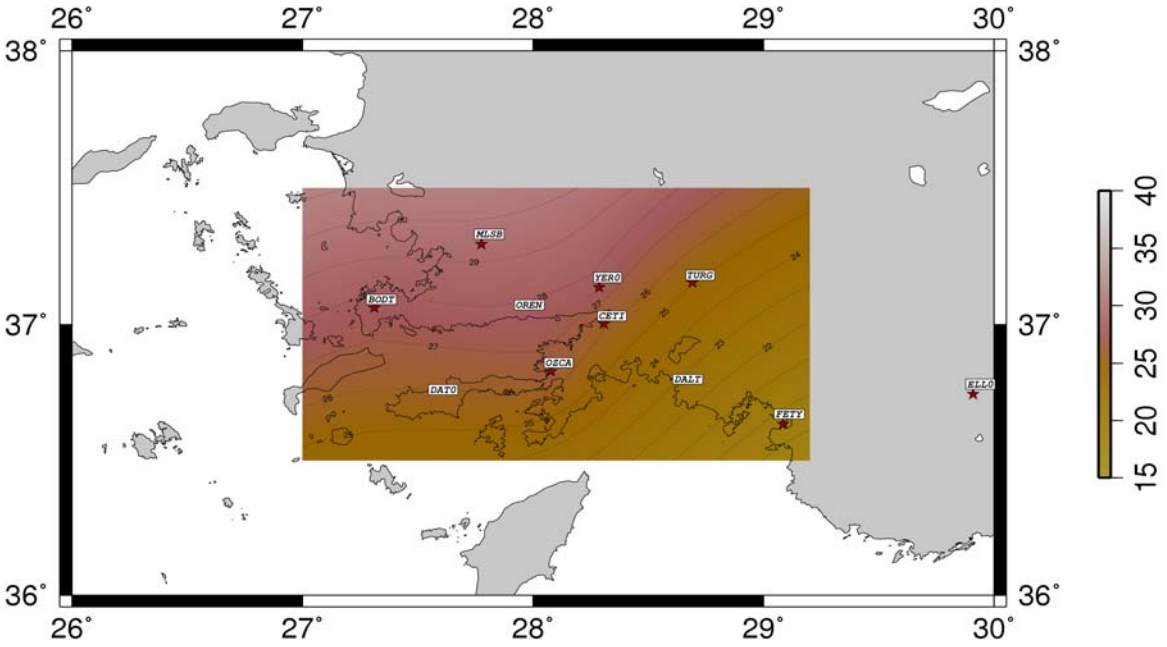

Figure 4.29. The depth map of Aegean Moho.
(Only depth at stations with star are used for the fitting)

Table 4.2 illustrates the depth of the African Moho which are estimated using the secondary conversion which do not correspond to any multiple. The value for Kappa is assumed to be equal to the generic one found above (K=1.78). An average velocity of Vp=6.2 Km/s is assumed for the propagation medium. It is clear that this assumption is open to discussion because the propagation medium contains both the Aegean Crust, African Crust and whatever is squeezed in between (accretionary material, Upper Mantle Material, etc). However it should give a good indication of relative depths of African Moho beneath individual station.

A contour map is shown in Figure 4.30 to illustrate the variation of the African Moho topography across the study area. The African Moho depths were fitted by adjustable tension continious curvature surface gridding algorithm in GMT package (Wessel and Smith, 1998).

Table 4.2.The secondary phases, which are interpreted as African Moho.

	K	H	Tps
BLCB_2	1.78	38.91	5.099
CETI_2	1.78	53.25	6.978
ELL0_2	1.78	58.68	7.690
DALT_2	1.78	51.51	6.750
DAT0_2	1.78	64.86	8.500
OZCA_2	1.78	57.54	7.550

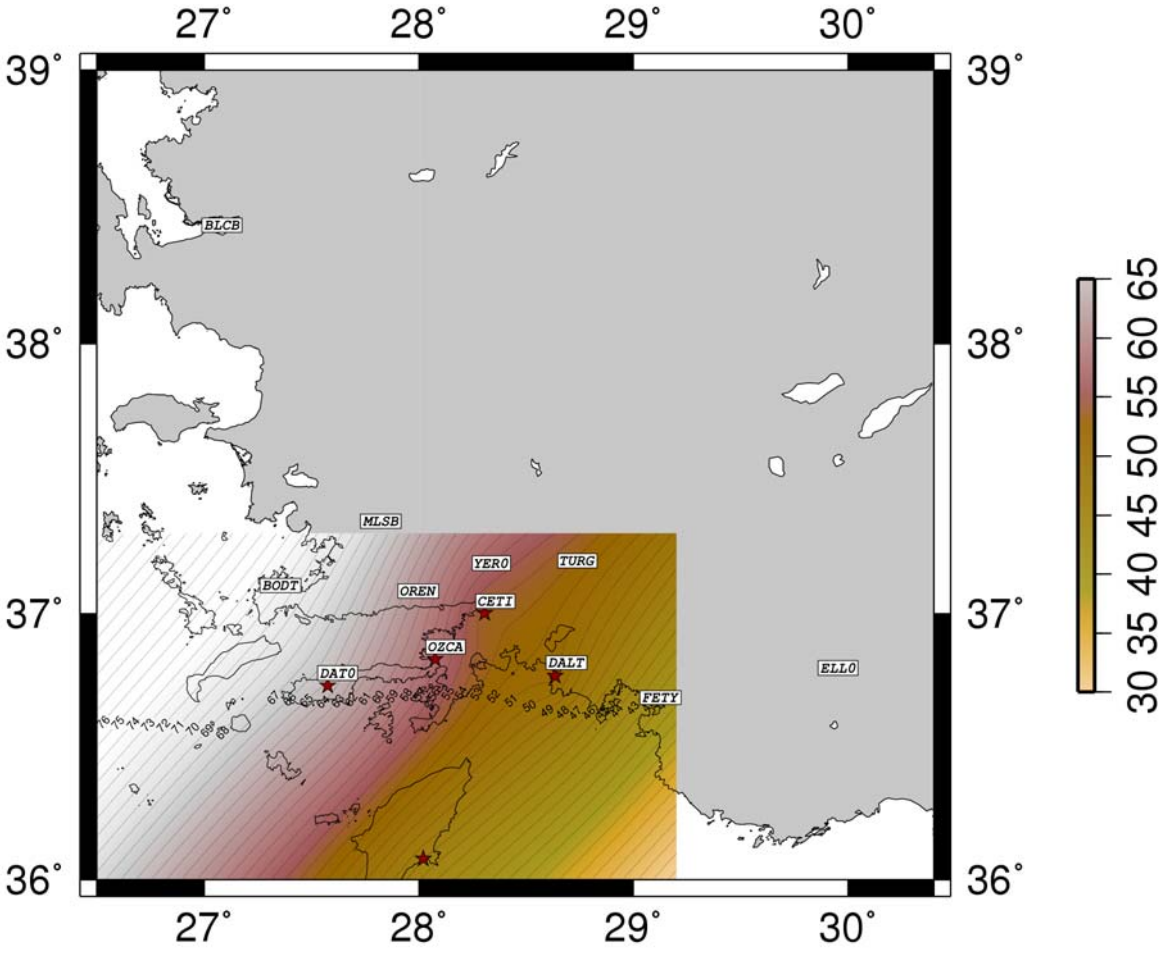

Figure 4.30. The depth map of African Moho.
(Only depth at stations with star are used for the fitting)

5. DISCUSSION AND CONCLUSION

Generally, the variation in incidence angle of the incoming seismic waves probably resulted in high dependence of receiver functions to distance and back azimuth of the events. However, major structures like Moho's of Aegean and African plates are still observable in most of the stations.

One major observation that needs to be made according to the results displayed in the previous chapter is that stations located in north and south of the Gökova Bay behave in a radically different way. In particular, stations that are on the north (MLSB, BODT, BLCB, TURG) give consistent Moho conversions with normal S-P delay times. Conversely, stations at the south of the Gökova Bay (DALT, DAT0, OZCA) fail to give a Moho conversion or give a sign of deeper interface. The stations that are located on the boundary of this transition (OREN, CETI, YER0) have a behavior somehow in between these two extremes. We may conclude that the Gökova Bay may constitute a major boundary at least at crustal scale between the north and the south. The normal fault that follows the axis of the Gökova Bay from east to west, probably defines the surface expression of this transition zone.

It can be noticed that the stations on the north exhibit normal continental crustal properties with sharp Moho transition located at a normally expected depth of 25-30 km. The fluctuations of the depth among these stations, is within the normal limit that one would expect from the wide scale Moho ondulations in western Turkey. This Moho topography is probably due to the intense tectonic activity that prevailed in the area and modified the shape of the continent. The whole of the continent that contituted the Aegean was first compressed intensely which probably thickened the crust and then stretched in NE-SW and N-S directions which, this time, caused the thinning of the crust. At this second stage, magmatism was also widely spread, which resulted in high amount of magmatic material to reach the surface and form mountain ranges, such as the Menderes Massif. We therefore expect that the crust that forms the western Turkey carries in it, traces of both of these tectonic processes. How fast the crust adapted itself to a new

tectonic regime is a function of the viscosity of the lower crust. It has been recently shown that the lower crust viscosity in western Turkey is relatively high (Zhu *et al.*, 2006) which causes that traces of the past regimes are preserved for a longer periods. To conclude one can say that it is not surprising to observe some ondulations of the Moho topography in Western Turkey, as a sign of recent and ongoing intense tectonic deformation.

The station further east at Elmalı (ELL) is also a typical sign of the ongoing tectonic activity that is deforming the SW Anatolia. It shows a very thick crust of 34 km. which is a characteristic of a deep rooted orogenic belt represented by The Taurus Mountains in this case. In fact, the station ELL is located at an altitude of about 1500 m, at the center of a high plateau that is formed by Lycian Taurus Mountains. We therefore conclude that the inferred deep crust of 34.3 km is in good agreement with the orogenic belt on which it is located.

The stations south of the Gökova Bay do not exhibit a clear Aegean Moho conversion in most cases. This is not an artifact of waveform processing or due to any insufficiency of data, because we see other well resolved conversions from deeper discontinuities on the same Figure, such as the one at 8-9 sec at DAT0. It is likely that this part of SW Anatolia, separated by the Gökova Bay from the North, constitute an abrupt E-W transition band between the relatively more stable continental crust in the north, to the highly deformed zone of subduction in the south. The fact that no clear Moho reflection was observed may be due to various reasons. The serpentinization and hydration in Upper Mantle can lower the sub-Moho velocity and therefore make the Moho transition more subtle. The presence of a complex geometry of non-horizontal reflecting surfaces, or a high degree of anisotropy in the crust, is also among the causes for not obtaining a clear Moho reflection. Both of these effects may be further tested by applying a finer application of the receiver function technique, which will take into account the azimuth and the distance of the incoming ray. However, at present time the data available do not allow such advanced technique. We simply state that the region south of Gokova Bay may behave in a similar fashion to Western Crete where Moho reflections are not clearly observed.

The Aegean Moho Map that is generated by surface fitting gives a rough picture of the general trend of the Moho topography. The variation of Moho depth indicates that the Crustal thickness of SW Turkey increases in NW direction. The direction of steepest descent agrees well with the work of Sodoudi *et al.* (2006). The thickness however has an offset of 2-4 kilometers. Comparing the number of stations from which the Moho map is generated, the map in this study is probably more accurate for this region.

The receiver functions which were obtained also give conversions from the subducting African plate. In stations which lie to the north of the Gökova bay, there is often only one conversion phase, which corresponds to the Aegean Moho conversion (except at BLCB where there is two conversions). This could indicate that either the conversion phase from African plate is too weak in these regions or it coincides with the multiple of Moho discontinuity of Aegean Crust. Probably both are true up to some extend. As far as the station BLCB is concerned, the deep conversion which arrives at 5.1 s is unlikely to correspond to an Aegean Moho multiple which we expect to arrive at about 9.0-13.0 s. It is also unlikely that this corresponds to an African Moho which, in this latitude, we expect to occur at around 9.5-10.0 second. A similar conclusion is drawn for the deep conversion at TURG which is too shallow for an inferred African Moho at this location.

However, for stations which lie to the south of the Gökova bay, the deeper conversion which is observable could well be interpreted as the Moho of the subducted African plate. The second phase arrives between 6.75-8.5 seconds which rules out the possibility of corresponding to a Aegean Moho multiple (always at about 9.0-13.0 s). However at this latitude the African Moho conversion is expected to occur at about these values (Soudoudi *et al.,* 2006). The depth of this phase increases in NW direction, which is consistent with the results of tomographic study of Papazachos and Nolet (1997) and receiver functions of Sodoudi *et al.* (2006).

It is clear that this work constitute an attempt to estimate whether the receiver function method can be used as a tool for studying the deeper structure of SW Turkey, just like it has been succesfully done for the Aegean Sea, particularly in the context of the subduction process. The results obtained, although based on data which cover a period of

15 months, are satisfactory to give a good picture of both the Aegean and the African Moho beneath SW Turkey. The next step, which already started as the natural continuation of this thesis, is to following improvements:

(i). Extend the time coverage

(ii). Apply finer geometrical corrections.

(iii). Make use of the S Receiver Functions

APPENDIX A: LIST OF EVENTS USED IN THE ANALYSIS

Year	Month	Day	Time(HHMMSS.mm)	Latitude	Longitude	Magnitude	Depth(km)
2006	4	1	100219.57	22.87	121.28	6.2	9
2006	4	5	174315.63	-37.28	78.28	5.8	10
2006	4	6	175916.44	23.32	70.48	5.5	10
2006	4	7	150002.10	44.88	150.37	5.5	65
2006	4	10	062613.30	7.51	-36.93	5.7	10
2006	4	12	010658.69	56.4	163.99	6	28
2006	4	14	092740.10	35.31	89.67	5.6	10
2006	4	15	224054.09	22.8	121.36	5.9	17
2006	4	16	114856.99	30.24	138.57	5.7	431
2006	4	16	174615.94	4.6	125.38	5.7	184
2006	4	19	203648.33	2.65	93.24	6.2	30
2006	4	19	210542.99	31.61	90.41	5.7	33
2006	4	20	175040.45	34.86	139.21	5.6	22
2006	4	20	232502.15	60.95	167.09	7.6	22
2006	4	20	232803.90	60.87	167.01	6.1	10
2006	4	21	043243.82	60.53	165.82	6.3	9
2006	4	21	111415.33	61.35	167.52	6.1	12
2006	4	22	072157.95	61.2	167.32	5.8	10
2006	4	25	182617.15	1.99	97	6.3	21
2006	4	26	163853.65	4.55	95.99	5.5	73
2006	4	28	090526.03	23.96	121.57	5.6	8
2006	4	29	165806.32	60.49	167.52	6.6	11
2006	4	30	004310.59	44.5	102.39	5.7	10
2006	5	6	182650.54	-38.62	78.57	6	10
2006	5	7	141735.17	-36.81	78.54	6.1	10
2006	5	7	164508.21	-36.83	78.57	5.5	16
2006	5	8	091657.87	-4.84	102.36	5.9	42
2006	5	9	110222.22	60.78	165.86	5.8	10
2006	5	10	024251.03	52.51	-169.26	6.4	18
2006	5	11	172254.14	23.31	94.32	5.7	48
2006	5	12	081656.51	-5.57	105.39	5.5	17
2006	5	13	031142.94	5.51	94.44	5.9	45
2006	5	16	152825.92	0.09	97.05	6.8	12
2006	5	18	230444.99	54.63	163.86	5.7	30
2006	5	19	144424.90	-0.14	124.71	6.2	35
2006	5	22	111200.38	60.77	165.74	6.7	16
2006	5	22	130801.67	54.28	158.43	6.2	184
2006	5	26	225358.92	-7.96	110.45	6.3	12
2006	5	28	090012.45	19.16	121.18	5.6	23
2006	5	29	141050.27	-41.95	88.46	5.6	10
2006	6	5	062707.96	1.17	-28.07	6	10
2006	6	5	063431.80	1.02	-28.16	5.6	10
2006	6	9	231727.88	-47.75	32.61	5.9	22
2006	6	11	200126.31	33.13	131.14	6.3	139
2006	6	14	041842.51	51.75	177.08	6.4	14

Year	Month	Day	Time(HHMMSS.mm)	Latitude	Longitude	Magnitude	Depth(km)
2006	6	15	042802.29	1.45	126.3	5.6	27
2006	6	15	064948.83	45.39	97.35	5.8	9
2006	6	16	025617	1.28	121.8	5.6	25
2006	6	16	171040.30	40.35	143.71	5.6	30
2006	6	16	201921.39	40.33	143.61	5.5	28
2006	6	18	182802.25	33.03	-39.7	5.9	10
2006	6	20	100207.78	51.58	-130.47	5.6	10
2006	6	21	123452.68	6.94	92.45	5.9	16
2006	6	22	105311.57	45.42	149.34	6.1	95
2006	6	24	211500.92	-0.39	123.19	6.3	26
2006	6	27	023935.27	52.21	176.18	6.2	33
2006	6	27	180722.74	6.5	92.79	6.2	28
2006	7	1	193439.61	51.06	-179.31	5.5	41
2006	7	2	035356.49	51.71	176.93	5.8	8
2006	7	2	165800.86	51.19	-179.39	5.5	46
2006	7	2	172025.78	51.1	-179.36	5.6	49
2006	7	6	035753.46	39.13	71.82	5.7	24
2006	7	8	204000.98	51.21	-179.31	6.6	22
2006	7	9	041620.11	51.04	-179.17	5.5	19
2006	7	10	072137.88	-11.63	-13.43	5.5	10
2006	7	12	144445.96	-8.55	67.81	5.7	10
2006	7	12	230620.26	-17.64	65.77	5.5	10
2006	7	17	081928.75	-9.25	107.41	7.7	34
2006	7	17	083228.45	-9.28	107.35	5.6	17
2006	7	17	090017.70	-9.68	107.52	5.5	24
2006	7	17	090517.36	-9.88	107.89	5.7	10
2006	7	17	091304.96	-9.09	107.76	6.1	10
2006	7	17	100906.76	-9.03	107.73	5.9	10
2006	7	17	104431.93	-9.09	107.68	5.5	10
2006	7	17	110736.45	-9.51	107.65	5.8	35
2006	7	17	125212.63	-9.01	107.83	5.7	23
2006	7	17	154202.60	-9.53	107.71	5.5	12
2006	7	17	154559.82	-9.42	108.32	6.1	21
2006	7	17	160955.05	-9.37	108.77	5.8	26
2006	7	17	194833.27	0.19	119.7	5.5	71
2006	7	17	194933.24	-9.06	107.86	5.5	11
2006	7	18	001548.64	-9.3	108.75	5.7	20
2006	7	18	032750.38	-0.17	124.96	5.8	21
2006	7	18	041823.28	-9.35	108.78	5.6	13
2006	7	19	015855.18	-9.22	108.37	5.5	10
2006	7	19	072506.36	-9.54	107.24	5.7	10
2006	7	19	105736.88	-6.53	105.39	6.1	45
2006	7	23	082204.16	-0.34	123.29	5.9	28
2006	7	25	123923.83	-9.26	108.41	5.6	10
2006	7	27	111640.37	1.71	97.15	6.1	20
2006	7	28	074013.75	24.19	122.53	5.9	49
2006	7	29	001151.34	37.26	68.83	5.6	34
2006	7	29	195343.05	23.59	-63.92	5.8	10
2006	7	30	012814.69	1.46	97.18	5.6	30
2006	8	2	144504.63	-11.17	116.85	5.9	15

Year	Month	Day	Time(HHMMSS.mm)	Latitude	Longitude	Magnitude	Depth(km)
2006	8	4	134139.83	9.97	-70.65	5.5	14
2006	8	6	142619.34	37.37	74.73	5.6	11
2006	8	6	181640.17	26.12	144.01	6	23
2006	8	11	205414.37	2.4	96.35	6.2	22
2006	8	12	183918.14	28.79	130.01	5.6	28
2006	8	14	130935	19.02	-64.64	5.5	21
2006	8	15	122617.35	51.09	179.26	5.7	19
2006	8	16	183900.37	-28.82	61.74	5.9	13
2006	8	17	111135.54	55.62	161.69	6.1	55
2006	8	17	152035.48	46.54	141.9	6	16
2006	8	20	030102.41	49.82	156.41	6	26
2006	8	24	215036.65	51.15	157.52	6.5	43
2006	8	26	234039.47	51.33	-179.57	5.8	35
2006	8	26	234618.52	51.38	-179.54	5.7	35
2006	8	27	171117.42	24.95	122.93	5.5	145
2006	8	29	105306.25	-0.35	125.12	5.8	36
2006	8	30	161339.71	-17.65	65.94	5.7	10
2006	8	31	080827.31	-0.27	125.06	6.1	35
2006	8	31	225825.80	28.8	130.03	5.6	33
2006	9	1	102517.13	53.26	159.7	5.7	51
2006	9	1	120422.17	53.97	-166.39	5.9	75
2006	9	5	045302.10	7.68	126.43	5.8	135
2006	9	6	050028.45	61.63	168.64	5.5	10
2006	9	9	041312.03	-7.21	120.11	6.3	571
2006	9	10	145608.16	26.32	-86.61	5.9	14
2006	9	11	181222.33	35.47	78.22	5.5	14
2006	9	12	155630.77	8.28	126.49	5.5	36
2006	9	16	022250.62	41.36	135.7	5.9	367
2006	9	16	061746.88	5.12	94.78	5.6	49
2006	9	17	073011.10	-17.69	41.83	5.5	10
2006	9	18	034558.91	51.51	-173.96	5.8	5
2006	9	19	135856.86	-9.9	107.35	5.9	12
2006	9	21	185450.05	-9.05	110.36	6	25
2006	9	24	225621.74	-17.74	41.81	5.7	10
2006	9	25	024337.20	-0.18	124.83	5.7	35
2006	9	28	013648.33	46.46	153.36	5.9	11
2006	9	29	130826.17	10.88	-61.76	6.1	53
2006	9	29	182305.94	10.81	-61.76	5.5	52
2006	9	30	124722.85	7.28	-34.66	5.6	10
2006	9	30	175023.05	46.35	153.17	6.6	11
2006	9	30	175616.10	46.19	153.17	6	10
2006	10	1	090602.32	46.47	153.24	6.6	19
2006	10	6	050853.74	-41.19	80.64	5.7	10
2006	10	9	100146.72	20.65	120.02	6.3	10
2006	10	9	110828.09	20.71	119.98	5.9	10
2006	10	9	181933.73	-51.03	29.02	5.7	10
2006	10	10	235804.17	37.2	142.66	6	10
2006	10	11	064353.81	20.71	120.08	5.7	10
2006	10	12	053035.38	4.94	95.01	5.5	30
2006	10	12	144630.93	24.13	122.62	5.7	44

Year	Month	Day	Time(HHMMSS.mm)	Latitude	Longitude	Magnitude	Depth(km)
2006	10	20	143100.15	13.43	121.47	5.8	22
2006	10	20	172703.25	13.49	121.53	5.8	25
2006	10	20	220927.35	13.42	121.55	5.6	10
2006	10	21	182320.98	13.37	121.38	5.9	18
2006	10	23	001921.20	4.95	125.22	5.7	10
2006	10	23	211719.98	29.35	140.27	6.4	11
2006	10	24	030345.28	4.9	125.29	6.1	10
2006	10	29	083144.60	29.37	140.2	5.6	10
2006	10	30	082741.74	2.32	126.78	5.6	36
2006	11	12	212742.44	48.28	154.25	6.1	36
2006	11	15	111413.57	46.59	153.27	8.3	10
2006	11	15	112306.92	46.3	154.61	5.6	10
2006	11	15	112429.86	46.27	154.52	5.6	10
2006	11	15	112457.49	47.77	153.18	5.5	10
2006	11	15	112509	47.52	152.65	6	10
2006	11	15	112838.46	46.09	154.1	6	10
2006	11	15	112922.79	46.37	154.48	6.2	10
2006	11	15	113323.80	46.86	153.73	5.5	10
2006	11	15	113458.13	46.65	155.3	6.4	10
2006	11	15	114055.05	46.48	154.73	6.4	10
2006	11	15	114804.23	44.1	154.7	5.5	10
2006	11	15	121605.54	47.11	154.42	5.7	10
2006	11	15	121644.15	46.19	154.67	5.9	10
2006	11	15	122615.76	47.42	153.86	5.7	10
2006	11	15	122821.33	47.06	155.53	5.5	10
2006	11	15	192525.99	47.01	154.98	5.6	10
2006	11	15	192806.39	47.08	155.17	5.5	10
2006	11	15	211708.22	46.87	155	5.5	10
2006	11	15	212221.46	47.28	154.15	6.1	12
2006	11	15	212522.53	47.14	153.51	5.7	10
2006	11	15	213124.32	47.38	154.16	5.5	13
2006	11	15	213509.59	47.67	154.55	5.6	10
2006	11	15	214008.55	46.72	153.3	5.5	10
2006	11	16	062020.77	46.36	154.47	6	9
2006	11	17	063349.45	47.02	155.53	5.6	10
2006	11	17	180312.26	28.59	129.9	6.2	22
2006	11	18	135521.15	4.75	94.78	5.9	32
2006	11	18	135753.78	4.74	94.77	5.9	29
2006	11	19	151652.20	46.9	154.89	5.6	10
2006	11	22	111509.62	44.15	146.78	5.6	79
2006	11	23	200446.60	47.54	154.2	5.7	10
2006	11	24	153410.17	46.76	153.77	5.7	11
2006	11	28	080151.76	46.69	155.53	5.6	10
2006	11	29	153844.50	53.74	-35.44	5.6	10
2006	12	1	035821.82	3.4	99.09	6.3	205
2006	12	1	140147.50	-8.25	118.78	6.3	43
2006	12	3	081951.31	-0.54	-19.74	5.6	10
2006	12	7	191021.85	46.15	154.39	6.3	16
2006	12	9	092446.75	5.08	94.75	5.5	30
2006	12	9	144855	47.44	147.02	5.8	405

Year	Month	Day	Time(HHMMSS.mm)	Latitude	Longitude	Magnitude	Depth(km)
2006	12	12	154803.27	3.73	124.68	6.3	213
2006	12	15	165902.39	46.41	153.04	5.7	10
2006	12	15	170109.58	46.39	153.06	5.5	10
2006	12	17	211021.91	4.82	95.02	5.8	36
2006	12	17	213917.45	0.63	99.86	5.8	30
2006	12	20	235555.88	13.27	125.81	5.6	24
2006	12	22	195044.63	10.65	92.36	6.3	24
2006	12	23	225940.53	-6.78	105.64	5.5	30
2006	12	25	200100.45	42.16	76.16	5.8	11
2006	12	26	122621.14	21.8	120.55	7.3	10
2006	12	26	123413.80	21.97	120.49	7.1	10
2006	12	26	124021.70	21.64	120.85	5.5	10
2006	12	26	151945.21	48.32	154.84	5.9	10
2006	12	26	154144.78	22.07	120.41	5.5	22
2006	12	27	023036.54	22	120.48	5.6	10
2006	12	30	083049.79	13.31	51.37	6.6	15
2007	1	5	165222.37	55.76	-156.06	5.8	18
2007	1	8	124840.51	8.08	92.44	6.2	11
2007	1	8	172150.28	39.8	70.31	6	18
2007	1	9	154935	59.37	-136.87	5.7	20
2007	1	11	203447.35	43.47	147.08	5.5	10
2007	1	13	042321.16	46.24	154.52	8.2	10
2007	1	13	043707.67	46.33	155.17	5.5	10
2007	1	13	091831.70	45.57	153.76	5.8	10
2007	1	13	173706.31	46.91	156.28	6	10
2007	1	13	193732.65	47.05	155.53	5.6	10
2007	1	15	181759.25	34.89	138.64	5.9	170
2007	1	16	180618.14	2.61	126.24	5.6	64
2007	1	17	231850.14	10.13	58.7	6.2	10
2007	1	18	152718.32	-5.49	101.45	5.9	17
2007	1	19	024423.42	-9.99	109.67	5.9	25
2007	1	21	112745.06	1.07	126.28	7.5	22
2007	1	21	115411.21	0.95	125.89	5.6	10
2007	1	21	123235.17	1.1	126.03	5.5	10
2007	1	21	143918.15	1.04	125.97	5.5	10
2007	1	21	173255.52	1.06	126.35	6.2	23
2007	1	21	195050.26	1.04	125.85	5.5	10
2007	1	21	234509.23	1.02	126.26	5.5	10
2007	1	25	105917.65	22.56	121.93	6	36
2007	1	27	102146.76	1.28	126.2	5.6	10
2007	1	28	120905.50	1.01	126.31	5.8	10
2007	1	31	203134.84	-7.82	107.19	5.6	51
2007	2	1	104326.72	1.22	126.35	5.5	10
2007	2	4	033319.39	35.34	-35.94	5.6	10
2007	2	4	205659.13	19.37	-78.52	6.2	10
2007	2	8	071504.71	46.48	153.24	5.5	10
2007	2	11	104735.01	6.18	94.4	5.6	67
2007	2	12	103521.17	35.8	-10.33	6.2	10
2007	2	12	124532.41	5.56	126	6.1	29
2007	2	13	192214.64	-0.44	124.19	5.5	84

Year	Month	Day	Time(HHMMSS.mm)	Latitude	Longitude	Magnitude	Depth(km)
2007	2	14	204631.93	0.64	97.23	5.6	4
2007	2	17	000256.76	41.79	143.55	6	31
2007	2	17	002227.49	41.77	143.6	5.6	35
2007	2	19	023344.40	1.76	30.75	5.6	28
2007	2	19	111303.49	5.56	126.24	5.5	29
2007	2	26	234953.73	-44.77	35.49	5.7	10
2007	3	1	020107	3.78	96.34	5.6	74
2007	3	1	231152.07	26.58	-44.59	5.9	10
2007	3	4	112611.98	33.79	-38.47	5.6	10
2007	3	6	034938.90	-0.49	100.5	6.4	19
2007	3	6	054926.92	-0.48	100.55	6.3	20
2007	3	7	105337.59	1.96	97.91	5.9	35
2007	3	8	050332.26	29.91	140.2	6.1	139
2007	3	9	032242.76	43.22	133.53	6.1	441
2007	3	9	072731.22	-11.43	66.25	5.8	10
2007	3	10	170337.86	74.26	8.71	5.7	10
2007	3	10	211258.47	55.23	161.91	5.9	37
2007	3	11	070926.41	43.99	147.89	6	49
2007	3	12	080759.69	-41.2	85.53	5.5	10
2007	3	12	185925.24	46.9	151.77	5.6	144
2007	3	13	090543.86	-8.13	117.86	5.6	10
2007	3	17	174226.29	1.13	126.22	6.2	35
2007	3	18	012524.11	42.16	144	5.6	35
2007	3	20	031030.47	9.19	126.12	5.5	35
2007	3	22	061043.09	-3.39	86.78	5.9	21
2007	3	25	004157.82	37.34	136.59	6.8	8
2007	3	26	072755.83	22.04	142.98	5.5	10
2007	3	26	165103.02	0.83	125.91	5.5	10
2007	3	27	121359.50	48.25	154.2	5.5	30
2007	3	28	211710.65	-6.27	29.67	5.8	8
2007	3	30	090505.69	44.14	146.01	5.5	100
2007	3	31	193717.84	1.27	122.63	5.6	27
2007	4	1	025105.30	32.35	137.61	5.7	378
2007	4	2	194256.16	1.41	125.76	5.8	55
2007	4	3	033507.28	36.45	70.69	6.2	222
2007	4	4	195803.80	-17.23	66.79	5.9	10
2007	4	4	214018.77	30.93	141.67	5.7	9
2007	4	5	035650.48	37.31	-24.62	6.3	14
2007	4	7	052049.63	-39.79	46.18	5.9	10
2007	4	7	070925.37	37.31	-24.49	6.1	8
2007	4	7	095151.62	2.92	95.7	6.1	30
2007	4	9	101804.58	48.3	154.7	5.8	36
2007	4	10	135653.89	12.99	92.53	5.5	30
2007	4	15	041230.19	47	153.43	5.6	34
2007	4	18	150731.60	42.66	141.86	5.5	119
2007	4	20	002640.60	25.72	125.09	6.1	10
2007	4	20	003059.96	25.73	125.15	5.7	10
2007	4	20	014556.11	25.71	125.11	6.3	9
2007	4	20	022334.04	25.62	125.04	5.9	11
2007	4	20	052311.28	25.68	125.24	5.5	10

Year	Month	Day	Time(HHMMSS.mm)	Latitude	Longitude	Magnitude	Depth(km)
2007	4	21	003224.85	21.14	122.13	5.5	10
2007	4	25	115255.62	7.4	126.44	5.6	27
2007	4	27	080249.65	5.36	94.64	6.3	38
2007	4	29	124157.39	52.01	-179.97	6.2	117
2007	4	30	153852.54	-54	6.08	5.6	10
2007	5	4	120652.21	-1.41	-14.91	6.2	10
2007	5	5	085139.09	34.25	81.97	6	9
2007	5	7	115947.56	31.35	97.79	5.6	12
2007	5	14	093143.10	1.25	97.25	5.5	30
2007	5	16	085616.47	20.5	100.75	6.4	23
2007	5	16	101745.14	48.86	154.77	5.5	10
2007	5	18	155958.53	41.6	141.99	5.5	58
2007	5	23	044146.54	52.35	-31.81	5.7	10
2007	5	24	010625.53	-9.55	118.8	5.6	37
2007	5	30	202212.66	52.14	157.29	6.4	116
2007	6	2	213457.78	23.03	101.05	6.3	5
2007	6	14	144954.11	10.38	125.31	5.5	10
2007	6	15	184953.39	1.72	30.83	5.9	24
2007	6	16	011847.97	1.15	126.41	5.8	47
2007	6	23	081719.89	21.47	99.78	5.6	22
2007	6	24	002518.40	-55.65	-2.63	6.5	10
2007	6	26	222303.04	-10.49	108.15	6	10
2007	7	1	041207.75	43.66	144.73	5.8	130
2007	7	3	082600.81	0.71	-30.27	6.3	10
2007	7	8	185400.22	46.84	155.48	5.5	10
2007	7	13	215443.11	51.84	-176.28	6	35
2007	7	15	130800.81	52.48	-168.05	6.1	10
2007	7	15	132615.24	52.36	-168.01	5.8	10
2007	7	16	011322.37	37.53	138.45	6.6	12
2007	7	16	063740.43	37.5	138.47	5.7	15
2007	7	16	141737.34	36.81	134.85	6.8	350
2007	7	16	225823.39	7.18	-72.13	5.6	29
2007	7	17	141042.46	-2.73	36.36	5.9	8
2007	7	20	100652.04	42.91	82.38	5.6	10
2007	7	21	224413.59	38.94	70.49	5.6	10
2007	7	23	134002.16	23.67	121.63	5.6	40
2007	7	25	233731.52	7.16	92.52	6.1	15
2007	7	29	045436.71	53.64	169.7	6	25
2007	7	30	224205.63	19.31	95.61	6	14
2007	7	31	150735.32	27.34	126.9	5.9	10
2007	7	31	225531.12	-0.16	-17.8	6.2	11

REFERENCES

Aktar, M., H. Karabulut, S. Özalaybey, and D. M. Childs, 2007, "A Conjugate Strike-Slip Fault System Within the Extensional Tectonics of Western Turkey", *Geophysical Journal International*, Vol. 171, pp. 1363-1375.

Ammon, C. J., 1991, "The Isolation of Receiver Effects from Teleseismic P Waveforms", *Bulletin of Seismological Society of America*, 81, Vol. 6, pp. 2504 –2510.

Bohnhoff, M., J. Makris, D. Papanikolaou and G. Stravakakis, 2001, "Crustal Investigation of the Hellenic Subduction Zone Using Wide Aperture Seismic Data", *Tectonophysics*, Vol. 343, pp. 239-262.

Bourova, E., Kassaras, I., Pedersen, H. A., Yanovskaya, T., Hatzfeld, D. and Kiratzi A., 2005, "Constraints on Absolute S Velocities Beneath the Aegean Sea from Surface Wave Analysis", *Geophysical Journal International*, Vol. 160, pp. 1006-1019.

Burdick, L. J. and C. A. Ammon, 1977, "Modeling Crustal Structure Through the Use of Converted Phases in Teleseismic Body-Wave Forms", *Bulletin of the Seismological Society of America,* Vol. 67, No 3, pp. 677-691.

Clayton, R. W. and R. A. Wiggins, 1976, "Source Shape Estimation and Deconvolution of Teleseismic Body Waves", *Geophysical Journal of Royal Astronomical Society*, Vol. 47, pp. 151-177.

Clément, C., M. Sachpazi, P. Charvis, D. Graindorge, M. Laigle, A. Hirn and G. Zafiropoulos, 2004, "Reflection-Refraction Seismic in the Gulf of Cornith: Hints at Deep Structure and Control of the Deep Marine Basin", *Tectonophysics*, Vol. 391, pp. 97-108.

Delibasis, N., J. Makris and J. Drakopoulos, 1988, "Seismic Investigation of the Crust and the Upper Mantle in Western Greece", *Annal. Geol. Pays Hell.*, Vol. 33, pp. 69-83.

Drakatos, G. and J. Drakopoulos, 1991, "3-D Velocity Structure Beneath the Crust and Upper Mantle of the Aegean Sea Region", *Pure and Applied Geophysics*, Vol. 135, pp. 401-420.

Gautier, P., J. P. Brun, R. Moriceau, D. Sokoulis, J. Martinod and L. Jolivet, 1999, "Timing, Kinematics and Cause of Aegean Extension, A Senario Based on A Comparison With Simple Analogue Experiments", *Tectonophysics,* Vol. 315, pp. 31–72.

Hatzfeld, D., 1989, "The Hellenic Subduction Beneath the Peloponnesus: First Results of A Microearthquake Study", *Earth Planet. Sci. Lett.* Vol. 93, 283–291.

Jackson, J., J. Haines and W. Holt, 1994, "A Comparison of Satellite Laser Ranging and Seismicity Data in the Aegean Region", *Geophysical Research Letters*, Vol.21, pp. 2849-2852.

Karagianni, E. E., C. B. Papazachos, Panagiotopoulos, P. Suhadolc, A. Vuan and G. F. Panza, 2005, "Shear Velocity Structure in the Aegean Area Obtained By Inversion of Rayleigh Waves", *Geophysical Journal International,* Vol.160, pp. 127-143.

Knapmeyer, M. and H. P. Harjes, 2000, "Imaging Crustal Discontinuities and the Downgoing Slab Beneath Western Crete", *Geophysical Journal International*, Vol.143, pp. 1-21.

Le Pichon, X. and J. Angelier, 1979, "The Hellenic Arc and Trench System: A Key to the Neotectonic Evolution of the Eastern Mediterranean Area", *Tectonophysics*, Vol. 60, pp. 1-42.

Li, X., Bock, G., A. Vafidis, R. Kind, H. P. Harjes, W. Hanka, K. Wylegalla, V. D. Meijde, M., and Yuan, X., 2003, "Receiver Function Study of the Hellenic Subduction Zone: Imaging Crustal Thickness Variations and the Oceanic Moho of the Descending African Lithosphere", *Geophysical Journal International*, Vol. 155, pp. 733-748.

Ligorria, J. P. and C. J. Ammon, 1999, "Iterative Deconvolution and Receiver-Function Estimation", *Bulletin of Seismological Society of America*, Vol.89, No. 5, pp. 1395-1400.

Makris, J. and C. Stobbe, 1984, "Physical Properties and State of the Crust and Upper Mantle of the Eastern Mediterranean Sea Deduced from Geophysical Data", *Marine Geology*, Vol.55, pp. 347-363.

Makris, J., 1973, "Some Geophysical Aspects of the Evolution of the Hellenides", *Bulletin of Geological Society of Greece*, Vol.10, pp. 206-213.

Makris, J., 1978, "The Crust and Upper Mantle of the Aegean region from Deep Seismic Soundings", *Tectonophysics*, Vol.46, pp. 269-284.

McKenzie, D. P., 1972, "Active Tectonics of the Mediterranean Region", *Geophysical Journal of Royal Astrophysical Society*, Vol.30, pp. 109-185.

McKenzie, D. P., 1978, "Active Tectonics of the Alpine-Himalayan Belt: the Aegean Sea and Surrounding Regions", *Geophysical Journal of Royal Astronomical Society*, Vol.55, pp. 217-254.

Mercier, J. L., E. Carey, H. Philip and D. Sorel, 1977, "La Neotectonique Plio-Quaternaire de I arc Egeen Externe et de la mer Egee et ses Relations Avec la Sismicite", *Bulletin de la Société Géologique de France*, Vol.18, pp. 159-176.

Nyst, M., and W. Thatcher, 2004, "New Constraints on the Active Tectonic Deformation of the Aegean", *Journal of Geophysical Research*, Vol.109, pp. 163 196.

Özalaybey, S., M. K. Savage, A. F. Sheehan, J. N. Louie, and J. N. Brune, 1997, "Shear-Wave Velocity Structure in the Northern Basin and Range Province from the Combined Analysis of Surface Waves and Receiver Functions", *Bulletin of Seismological Society of America*, Vol. 87, pp. 183-199.

Panagiotopoulos, D. G. and Papazachos, B. C., 1985, "Travel Times of Pn Waves in the Aegean and Surrounding Area", *Geophysical Journal of Royal Astrophysical Society*, Vol. 80, pp. 165-176.

Papazachos, C. B. and G. Nolet, 1997, "P and S Deep Velocity Structure of the Hellenic Area Obtained By Robust Nonlinear Inversion of Travel Times", *Journal of Geophysical Research*, Vol.102, pp. 8349-8367.

Papazachos, C. B., P. M. Hatzidimitriou, D. G. Panagiotopoulos and G. N. Tsokas, 1995, "Tomography of the Crust and Upper Mantle in Southeast Europe", *Journal of Geophysical Research*, Vol.100, pp. 12405-12422.

Sodoudi, F., R. Kind, D. Hatzfeld, K. Priestley, W. Hanka, K. Wylegalla, G. Stavrakakis, A. Vafidis, H. P. Harjes and M. Bohnhoff, 2006, "Lithospheric Structure of the Aegean Obtained from P and S Receiver Functions", *Journal of Geophysical Research*, Vol.111, pp. 504-527.

Spakman, W., 1986, "Subduction Beneath Eurasia in Connection With the Mesozoic Tethys", *Geologie en Mijnbouw*, Vol.65, pp. 145-153.

Spakman, W., S. Van der Lee and R. D. Van der Hilst, 1993, "Travel Time Tomography of the European-Mediterranean Mantle Down to 1400 Km", *Physics of the Earth and Planetary Interiors*, Vol.79, pp. 3-74.

Spakman, W., M. J. R. Wortel and N. S. Vlaar, 1988, "The Hellenic Subduction Zone: A Tomographic Image and its Geodynamical Implications", *Geophysical Research Letters*, Vol.15, pp. 60-63.

Şengör, A.M.C., M. Satır and R. Akkok, 1984, "Timing of Tectonic Events in the Menderes Massif, Western Turkey: İmplications For Tectonic Evolution and Evidence For Pan-African Basement in Turkey," *Tectonics,* Vol.3, pp. 693–707.

Tiberi, C., M. Diament, H. Lyon-Caen and T. King, 2001, "Moho Topography Beneath the Corinth Rift Area (Greece) from Inversion of Gravity Data", *Geophysical Journal Internationsal*, Vol.145, pp. 797-808.

Tirel, C., F. Gueydan, C. Tiberi and J. P. Brun, 2004, "Aegean Crustal Thickness Inferred from Gravity Inversion Geodynamical Implications", *Earth and Planetary Science Letters*, Vol.228, pp. 267-280.

Tsokas, G. N. and R. O. Hansen, 1997, "Study of the Crustal Thickness and Subducting Lithosphere in Greece from Gravity Data", *Journal of Geophysical Research*, Vol.102, pp. 20585-20597.

Wessel, P. and W.H.F. Smith, 1998. "New Improved Version of the Generic Mapping Tools Released", EOS Trans. AGU 79, pp. 579.

Zhu, L. and H. Kanamori, 2000, "Moho Depth Variation in Southern California from Teleseismic Receiver Functions", *Journal of Geophysical Research*, Vol. 105, B2, pp. 2969-2980.

Zhu, L., J. B. Mitchell, N. Akyol, I. Cemen and K. Kekovali, 2006, "Crustal Thickness Variations in the Aegean Region and Implications For the Extension of Continental Crust", *Journal of Geophysical Research*, Vol.111, pp. 3469-3480.